SKB

TECHNICAL REPORT 88-23

Source parameters of major earthquakes near Kiruna, Northern Sweden, deduced from synthetic seismogram computation

W Y Kim, E Skordas, Y P Zhou, O Kulhanek

Seismological, Department, Uppsala University,
Box 12019, S-750 12 Uppsala

June 1988

SVENSK KÄRNBRÄNSLEHANTERING AB
SWEDISH NUCLEAR FUEL AND WASTE MANAGEMENT CO

BOX 5864 S-102 48 STOCKHOLM
TEL 08-665 28 00 TELEX 13108-SKB

SOURCE PARAMETERS OF MAJOR EARTHQUAKES NEAR KIRUNA, NORTHERN SWEDEN, DEDUCED FROM SYNTHETIC SEISMOGRAM COMPUTATION

W Y Kim, E Skordas, Y P Zhou, O Kulhanek

Seismological Department, Uppsala University, Box 120 19
S-750 12 Uppsala

June 1988

Source Parameters of Major Earthquakes near Kiruna, northern Sweden, deduced from Synthetic Seismogram Computation

Kim, W. Y., Skordas, E., Zhou, Y. P. and Kulhanek, O.

Seismological Department
Uppsala University
Box 120 19
750 12 Uppsala
Sweden

June, 1988

ABSTRACT

The earthquakes that have occurred around Kiruna in northern Sweden have been studied in detail in order to determine their source characteristics and to understand the pattern of seismic activity in the region. All earthquakes with magnitude greater than 3.0 (M_L) that occurred during the period between 1967 and 1985 in the region bounded by 66.5° - 69° N and 19° - 25° E are studied.

Relocated epicenters of the events exhibit a cluster of events in a direction NE - SW at the western side of the region close to Kiruna. Though, the focal depths of the events are not very well constrained, the relocation results suggest that the events in this cluster might have occurred at focal depths between 15 and 25 km.

At the eastern side of the region, the epicenters are roughly aligned along an elongated area trending NNW - SSE. The focal depths of the events in this area tend to be shallow and are probably in the upper crust at the depths range from 5 to 16 km.

The earthquakes studied show nearly constant source radii of about 0.4 ~ 0.6 km over the seismic moment range 10^{20} to 10^{21} dyne-cm. Consequently, the events studied are characterized by a steadily increasing stress drop relative to increasing seismic moment.

The source mechanisms obtained for the two largest earthquakes suggest that the mechanisms are dominated by the normal faultings on the near-vertical fault planes trending N-S to NE - SW.

TABLE OF CONTENTS

SUMMARY

The main objective of this work is to determine the seismic source parameters, such as seismic moment, source radius and stress drop, as well as to estimate the focal depth and source mechanism of earthquakes which have occurred around Kiruna, in northern Sweden and to study the seismicity of the region in detail.

All earthquakes with magnitude greater than M_L = 3.0 that occurred in the source region during the past 25 years are selected for the analysis. The source region under study is a typical intra-plate region with low seismicity characterized by the occurrence of small crustal earthquakes.

The major problem to study the seismicity of the region is that the events in question are small. Thus, they are recorded by only a few short-period seismograph stations operating at regional distance (Δ = 100 ~ 500 km). Hence, it is very difficult to determine the source parameters reliably due to the lack of good quality data.

In order to study the characteristics of the events, all available seismogram data have been collected and digitized for quantitative analysis. The data set consists of three-component short-period seismograms recorded by stations in Finland, Norway and Sweden. Altogether, about 200 seismograms are collected and photographically enlarged for further analysis and digitizing. The enlarged seismograms are digitized by using a data aquisition system which consists of an electronic digitizing table and a personal computer with high resolution graphic display screen. The digitizing table has a resolution limit of about 0.125 mm and it converts analog seismogram traces into digital form suitable for quantitative analysis.

For the 14 events studied, arrival times of the major crustal phases, such as Pn, Pg, Sn and Sg, are measured and the events are relocated by using the method of Joint Hypocenter Determination.

Spectral analyses of Lg waves on vertical-component seismograms are performed to determine the source parameters. Three-component digitized seismograms are analysed and corresponding synthetic seismograms are calculated to constrain the focal depth and source mechanism.

Results of the relocation revealed that the epicenters of the earthquakes are clustered in two regions. These clusters are likely associated with the fault plane determined in the source mechanism.

1. INTRODUCTION

The current seismic activity in Sweden is relatively low and characterized by the occurrence of only small earthquakes. Most of the instrumentally recorded earthquakes in Sweden are below magnitude 4 (M_L) and their distribution does not show any clear lineament. Nevertheless, the seismic activity recorded during the past 25 years, or so, reveals several regions in Sweden with somewhat higher seismicity than in surrounding areas (see Figure 1-1). From the south to the north, these regions are:

- lake Vänern region extending to the coast along Kattegat in the south,
- an elongated region along the coast of the Gulf of Bothnia,
- region around Kiruna, in northern Sweden, including also the area along the border between Sweden and Finland to the east.

In the present work, we study the earthquakes which have occurred around Kiruna and along the Swedish-Finnish border. The source region under study is bounded by 66.5° - 69°N in latidude and 19° - 25°E in longitude. The distribution of epicenters in the region shows a rather diffuse seismicity when compared with the Bothnian and Lake Vänern seismic zones.

Source properties of the earthquakes in the considered source region are studied in detail in an attempt to improve our knowledge of the event characteristics and our understanding of the seismotectonics of the region. During the period between 1961 and 1986, fourteen earthquakes with magnitude greater than 3.0, but not exceeding magnitude 4.0 have occurred in the source region. These earthquakes, typical small intra-plate events, provide the only clue to the current tectonics of the region. They are exclusively recorded by a few analog seismograph stations at distances ranging from 100 km to 500 km. Thus, it is difficult to determine the source characteristics of these events mainly due to the lack of high quality data. In the present work, we employed the complete synthetic seismograms calculated for a seismic source embedded in a layered crust to deduce the source properties.

In Section 2, we relocate the earthquake hypocenters by using the arrival times of major crustal phases read directly from original records. A precise location of the epicenters is essential for a correct intrepretation of the current seismic activity and for infering a possible correlation between the occurrence of earthquakes and the tectonic lineaments in the region.

In Section 3, seismic source parameters such as, seismic moment, source radius and stress drop, are determined from an Lg-wave spectral analysis.

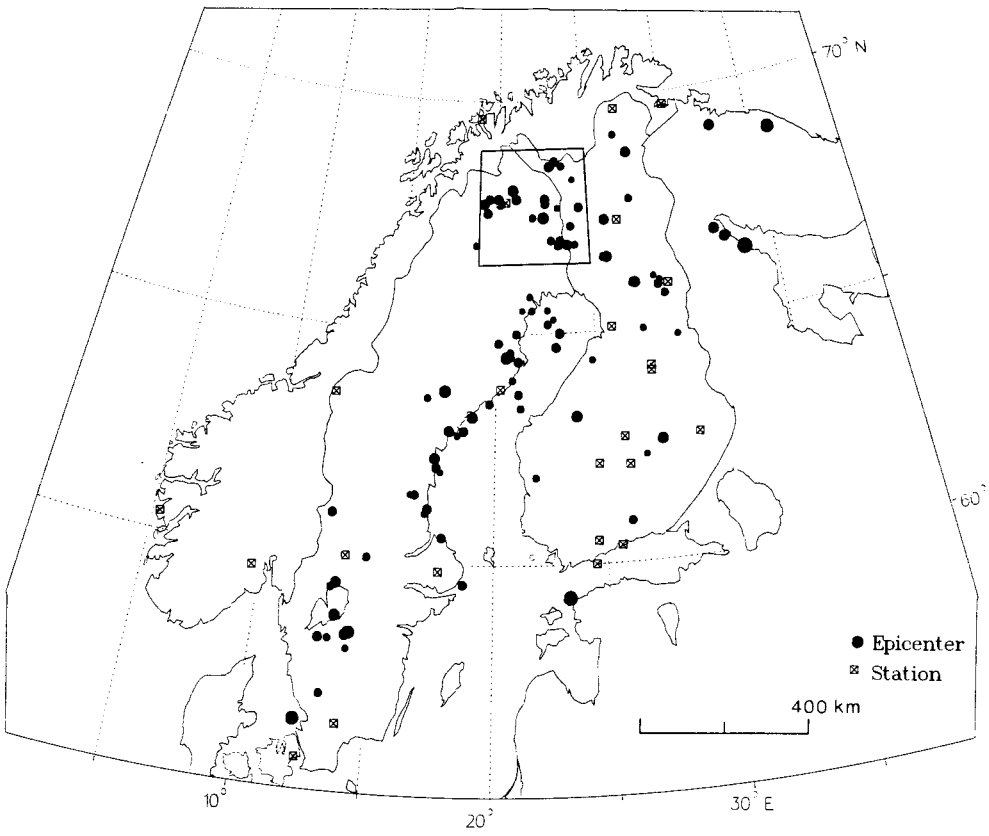

Figure 1-1. Epicentral distribution of earthquakes in the Fennoscandian shield, 1961-1986 and locations of seismograph stations (squares). All events with magnitude greater than 3.5 (M_L) are plotted and some of the events within the magnitude range 2 to 3.4 are included. Solid circles denote epicenters and their sizes are proportional to the magnitude of the events. Note that the solid circle given in the legend corresponds to magnitude 4. The inset indicates the northern Sweden seismic zone, bounded by 66.5° - 69°N in latitude and 19° - 25°E in longitude.

Finally, focal depths and source mechanisms of the events are further constrained by calculating the synthetic seismograms and by comparing them with corresponding observed records.

2. RELOCATION OF EARTHQUAKES

The source region under study is located at the northern extention of the Bothnian seismicity zone in northern Sweden, where the earthquake epicenters are concentrated in an elongated region trending NE-SW along the coast line of the Gulf of Bothnia (see Figure 1-1).

2.1 Previously Known Epicenters

Previously known epicenters around Kiruna, given by the Uppsala monthly bulletins, are listed in Table 2-1 and also depicted in Figure 2-1. As shown in the figure, some epicenters appear to be weakly clustered around Kiruna at the western border of the source region, whereas in the eastern part of the region, the epicenters are distributed along the NNW - SSE direction. However, the epicentral distribution does not suggest any clear lineaments (Figure 1-1 and Figure 2-1).

Table 2-1 Major Earthquakes around Kiruna, northern Sweden.

Event no.	Date	Origin time (h m sec)	Epicentral coordinates (^{o}N)	(^{o}E)	Magnitude (M_L)
1	04 Jan. 1967	04 44 18	67.9	21.0	3.2
2	13 Apr. 1967	08 46 19	68.1	20.8	3.7
3	4 Sept.1968	17 09 14	66.9	23.8	3.4
4	4 Jul. 1969	22 28 54	67.6	19.4	3.1
5	17 Apr. 1971	08 05 03	67.8	22.6	3.1
6	17 Apr. 1973	06 17 59	67.9	20.0	3.3
7	1 Dec. 1974	19 35 58	67.8	20.1	3.2
8	11 Aug. 1975	18 28 09	67.5	22.5	3.9
9	16 Jan. 1978	02 28 24	67.9	22.6	3.2
10	28 May 1980	10 36 45	67.7	24.5	3.1
11	31 Jan. 1982	03 38 51	68.7	23.2	3.1
12	4 Jan. 1983	20 51 04	68.6	22.9	3.4
13	25 Aug. 1984	19 39 14	67.9	19.5	3.1
14	2 Apr. 1985	19 29 40	66.9	23.3	3.2

Previously announced epicenters are poorly determined by means of instrumental analog data, due to few and unfavorably distributed seismograph stations with respect to northern Sweden. Focal depths of the earthquakes are unknown. Moreover, we found several errors in phase arrival data used in the previous epicenter determinations. Thus, we attempted to relocate the events, since, rather precise locations are required to examine the seismicity pattern in the region and to postulate a plausible regional tectonic model.

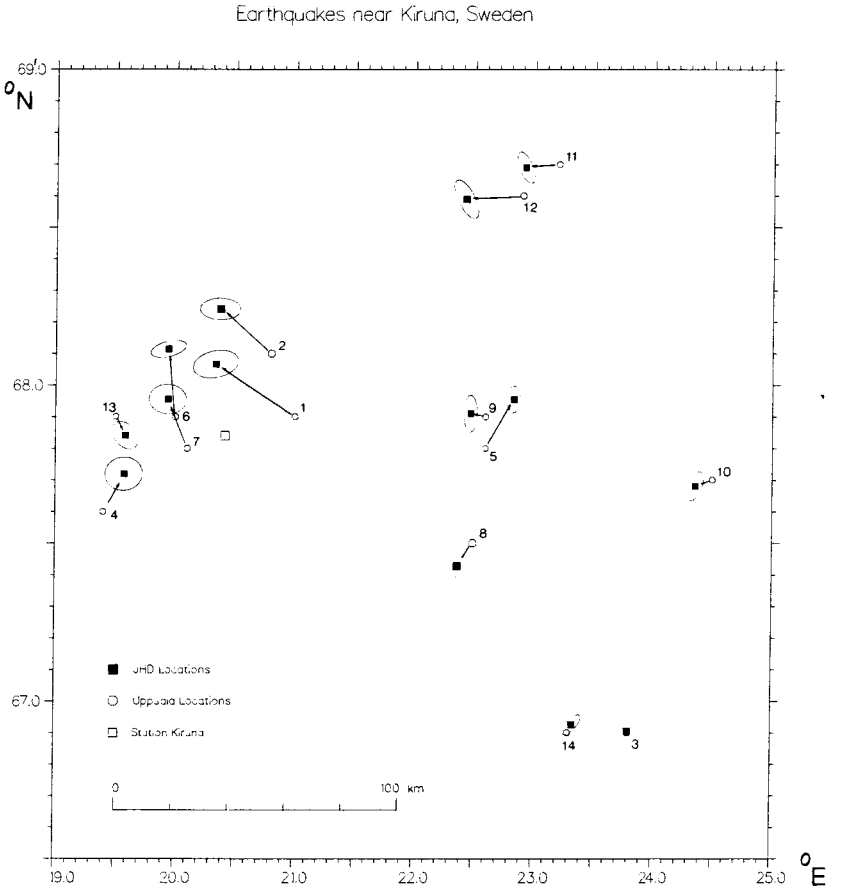

Figure 2-1. Epicenters of earthquakes that occurred between 1963 and 1986 studied in this report. Open circles denote epicenters previously assigned by the Seismological Department, Uppsala University and their numbers refer to the events nos. listed in Table 2-2. Squares correspond to the revised epicenters obtained with the JHD method. The ellipse around each relocated epicenter is the projection on the Earth's surface of the 90 percent confidence ellipsoid on the hypocenter. Mislocation vectors between Uppsala (tail) and JHD locations (head) are indicated.

2.2 Relocation of Earthquakes

We have relocated earthquakes in the source region by employing the method of Joint Hypocenter Determination (JHD). JHD minimizes location bias by applying constant station corrections to the travel-time curve. The JHD station corrections were computed specifically for a group of earthquakes in the region under study (Dewey, 1983; Engdahl et al., 1982).

In the JHD location procedure, first arriving P and S waves and Pg and Lg at regional distances were used. Velocities of the Pg and Lg phases are those derived by Båth (1971) for Sweden, namely 6.4 km/s and 3.6 km/s, respectively. Phase arrival times were read directly from the original seismograms recorded in Scandinavia (Finland, Norway and Sweden) by seismograph stations operating at the time of the earthquakes. The epicentral distance range of the stations were 20 km to 560 km. The stations used and their locations are listed in Table 2-2.

The essential features of the JHD location procedure we employed are the following:

- Travel time of a certain phase to a particular station is determined from the time predicted by the velocity model used minus a constant that is the same for all events in northern Sweden. This constant is associated with that particular phase at that particular station and is called the station-phase adjustment.

- After the station-phase adjustments were estimated for all stations, the hypocenters were determined for each earthquake using the JHD procedure.

- To make the set of normal equations for the hypocenter and the station adjustments well determined, the location of one event was held fixed in the computation. The event on 11 August 1975 (M_L = 3.9), being the largest among the events, has been used as such a calibration event. This earthquake provides the best arrival time data set and consequently, it is reliably located by the available observations.

Results of the epicenter relocations are listed in Table 2-3 and depicted in Figure 2-1. The accuracy of the epicenter locations determined in this study (Table 2-3) is significantly improved. All phase arrival times have been read by present authors from original seismograms and consequently the arrival times used for the relocation are considered to be homogeneous with negligible reading errors.

The reliability of the relocated epicenters is given by the ellipses around each epicenter, which are the projection on the earth's surface of the 90-percent confidence ellipsoid on the hypocenter.

Table 2-2 Station Information*

Station code	Coordinates (^{o}N)	(^{o}E)	Distance (km)	Azimuth (^{o})	Instrument†
KEV	69.759	27.011	320.1	36	Benioff (3)
KIR	67.844	20.417	94.5	300	Grenet (Z)
KJF	64.209	27.725	433.8	145	Benioff (3)
MA	65.919	29.052	338.9	119	Willmore (Z)
NUR	60.515	24.652	777.3	171	Benioff (3)
OUL	65.087	25.905	304.6	148	Willmore (Z)
SKA	63.589	12.289	641.0	226	Grenet (Z)
SOD	67.374	26.637	182.2	91	Benioff (Z)
TRO	69.643	18.936	282.4	331	Benioff (Z)
UME	63.825	20.239	413.4	194	Benioff (3)
UPP	59.864	17.633	873.5	196	Benioff (3)

* Azimuth and distance are measured from the epicenter of the event on 11 Aug. 1975.

(†) (3) denotes three-component seismographs and (Z) indicates vertical-component only.

Note that the JHD locations are displaced from the Uppsala epicenters by up to 30 km (see Figure 2-1). It is not straight forward to attribute displacements in the epicentral locations as due to earth's structure. Since the number of stations is not sufficient and the station distribution is unfavorable for the location procedure, the relocated epicenters still tend to be mislocated in a direction approximately parallel with the gap in the azimuthal coverage of stations. The influence of the unfavorable station distribution is also reflected in the major axis of the confidence ellipses which point in the least resolved direction. As shown in Figure 2-1, at the western side of the source region, the epicenters of six events (event nos. 1, 2, 4, 6, 7 and 13) are clustered around the seismograph station, Kiruna (KIR). These earthquakes are roughly aligned in the NE-SW direction. Note that these events have relatively large location errors indicated by the size of the confidence ellipses. These relatively large errors are caused by a poor azimuthal coverage by observing stations for the six events.

Earthquakes that occurred in the eastern side of the region (event nos. 3, 5, 8, 9, 10, 11, 12 and 14) show smaller location errors when compared with those in the western side. This is mainly due to the improved azimuthal coverage by seismograph stations for these earthquakes (see Figures 1-1 and 2-1). The eastern-side earthquakes are aligned along the NNW-SSE direction.

Table 2-3 Relocation of Earthquakes in northern Sweden

Event no.	Date	Origin time (h m s)	Epicentral coordinates (^{o}N)	(^{o}E)	Focal depth (km)
1	4 Jan. 1967	04 44 17.4	68.07	20.34	25.1
2	13 Apr. 1967	08 46 14.8	68.24	20.37	31.2
3	4 Sept.1968	17 09 14.9	66.90	23.80	11.8
4	4 Jul. 1969	22 28 53.8	67.72	19.57	19.9
5	17 Apr. 1971	08 05 00.9	67.96	22.84	16.0
6	17 Apr. 1973	06 17 54.8	68.11	19.94	0.1*
7	1 Dec. 1974	19 35 55.6	67.96	19.94	23.5
8	11 Aug. 1975	18 28 09.9	67.43	22.37	16.1
9	16 Jan. 1978	02 28 24.4	67.91	22.48	4.9
10	28 May 1980	10 36 45.0	67.68	24.36	9.2
11	31 Jan. 1982	03 38 54.0	68.69	22.92	26.9
12	4 Jan. 1983	20 51 04.1	68.59	22.42	20.7
13	25 Aug. 1984	19 39 14.3	67.84	19.58	5.2
14	2 Apr. 1985	19 29 40.0	66.93	23.34	37.8

* Depth is not determined and fixed at 0.1 km.

Computed focal depths for seven of the 14 studied earthquakes are in the upper crust. It is interesting to note that the earthquakes clustered around Kiruna have been located at focal depths between 15 and 25 km. This means that the hypocenters are placed near the upper and lower crust boundary (Conrad discontinuity). On the other hand, earthquakes in the eastern side of the source region, particularly those in the SE quadrant, had focal depths ranging from about 5 to 16 km, which will locate them into to the upper crust (see Table 2-3).

Focal depths listed in Table 2-3 are not well enough determined due to the contamination of arrival-time data by noise from various sources, such as for example, lateral heterogeneities in the crust and departures of the true seismic velocity model from the assumed one used in the location procedure. Focal depths of the earthquakes under consideration will be further constrained by using the synthetic seismogram calculation (see Section 4).

3. SEISMIC SOURCE PARAMETERS

Dynamic source parameters, such as seismic moment, stress drop and source radius for the earthquakes studied were determined from a spectral analysis of Lg waves. Altogether 47 Lg-wave short-period vertical-component seismograms recorded by stations in Sweden and Finland were selected for the analysis. The epicentral distances of Lg-wave data were in the range of 90 km to 900 km.

3.1 Lg-wave Spectral Analysis

3.1.1 Data

The instrument responses of stations providing short-period analog records differ from station to station. Six stations were equipped with WWSSN or equivalent Benioff (KEV, KJF, NUR, SOD, UME and UPP), two stations with Grenet (KIR and SKA) and another two with Willmore Mark-II (OUL and MA) short-period seismographs. Station information and instruments used are given in Table 2-2. Although, few stations had instrument responses with good sensitivity beyond about 10 Hz, reponses of the most stations were typically of WWSSN short-period types. The use of analog seismograms imposed limits on the reliable frequency range to about 5 Hz.

Selected seismograms were photographically enlarged three to five times and portions containing Lg waves were digitized on an electronic digitizing table. The digitized data were detrended for linear trend and interpolated for equal-time intervals of 0.05 s by using the piecewise continuous cubic polynomial (Wiggins, 1976). The corresponding Nyquist frequency of 10 Hz was adequate with respect to the frequency contents of the observed Lg waves. Records from large events (magnitude greater than 3.5) made at short epicentral distances could not be used due to their extremely high frequency contents and several missing traces on the available analog records.

3.1.2 Method of Spectral Analysis

The digitized seismograms were Fourier transformed to obtain trace amplitude spectra. The time window used for the spectral analysis of Lg waves varied from about 15 to 30 s depending upon the distance and size of the earthquakes. The observed Lg-wave amplitude spectra were corrected for instrument reponses to obtain estimates of the ground displacement spectra. To minimize the influence of noise, the spectra were considered only in the frequency band, for which the instrument response was greater than nine-tenth its peak magnification. This criterion limits the available frequency range for the spectral analysis to between about 0.3 and 8 Hz for most of the instruments used. However, in some cases, the displacement amplitude spectra became unreliable already for frequencies beyond about 5 Hz.

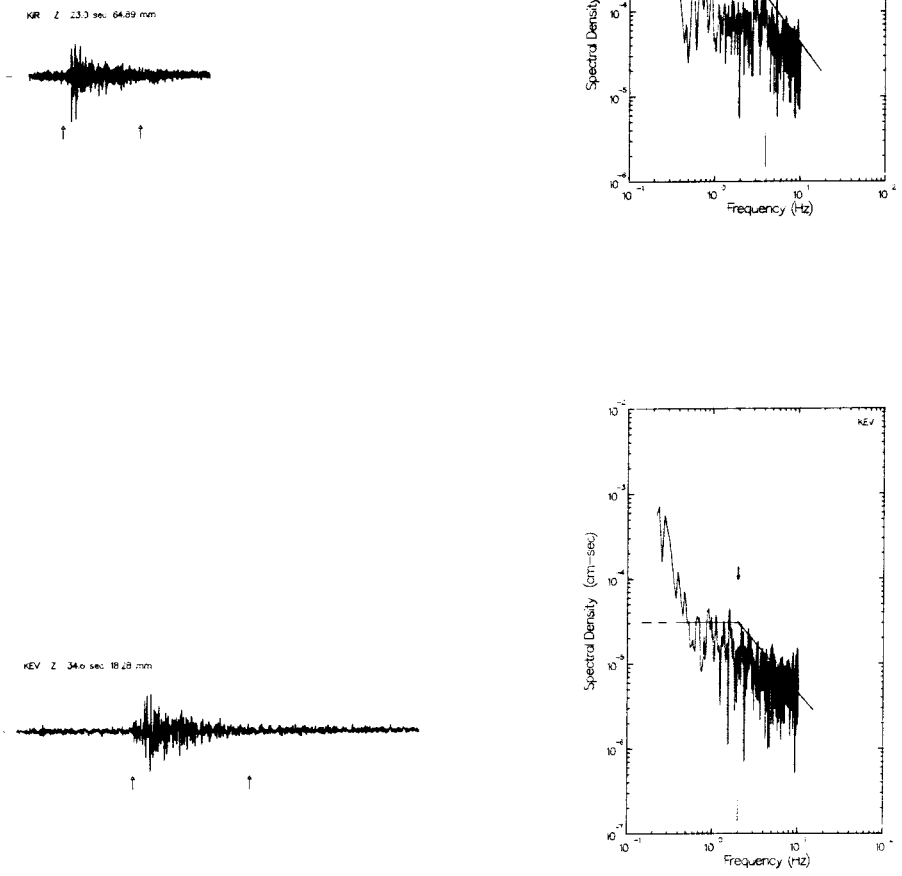

Figure 3-1a. Digitized seismograms (left) and corresponding ground displacement amplitude spectra (right) for the event of 11 August 1975 (M_L = 3.9). Time window used for spectral analysis is indicated by upward arrows below the seismogram traces. Choices of the low-frequency spectral level and the high-frequency asymptote are indicated by straight line segments and the corner frequency is denoted by a downward arrow in the spectrum. Station code, component, window length and peak-to-peak amplitude are given above each trace.

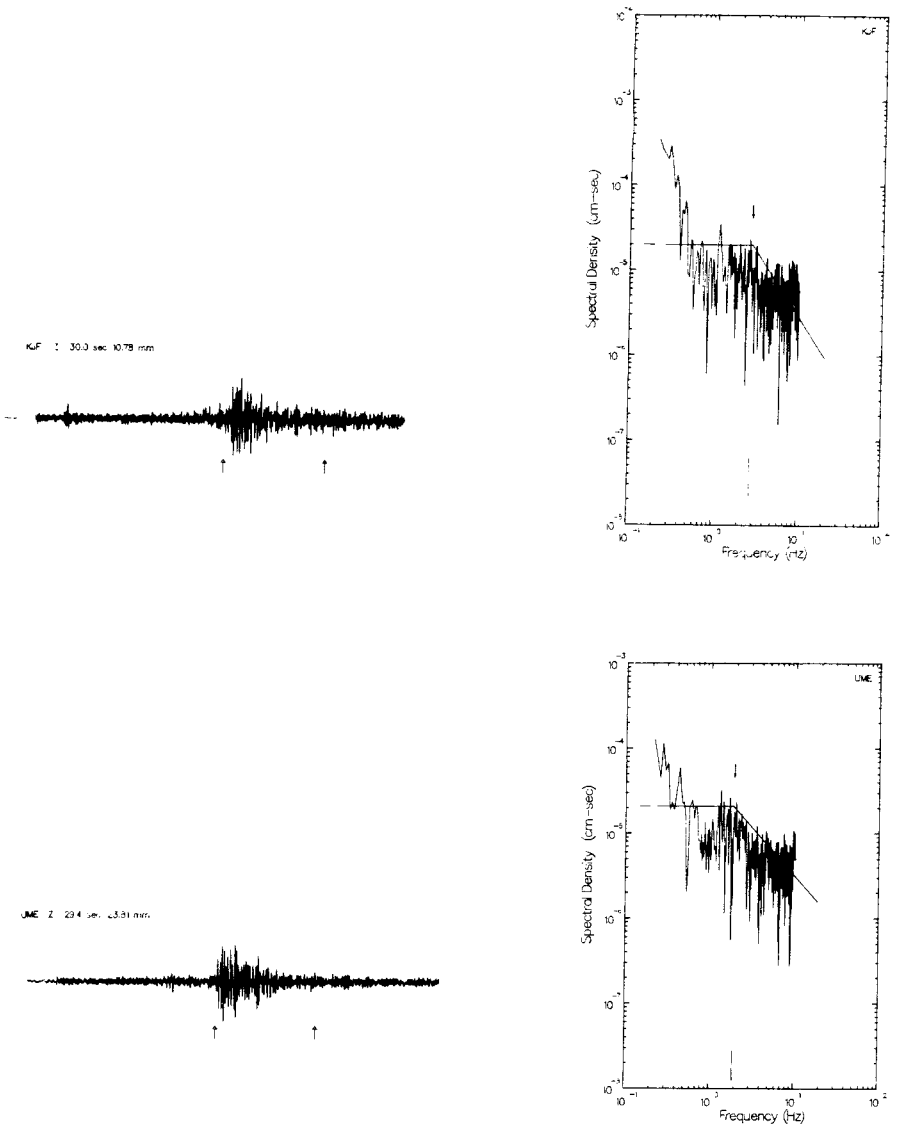

Figure 3-1b. Digitized seismograms (left) and corresponding ground displacement amplitude spectra (right) for the event of 11 August 1975 (M_L = 3.9). Other notations are the same as in Figure 3-1a.

Corrected displacement amplitude spectra were used to determine the constant low-frequency spectral level (Ω_o) and corner frequency (f_R). Two examples of ground displacement amplitude spectra and corresponding seismograms with time window used are shown in Figure 3-1. In the figure, the Lg-wave amplitude spectra fall off with increasing frequency, f, as f^{-2}. This asymptotic trend in the high-frequency portion of the spectrum is indicated in the figures by dashed lines.

3.1.3 Determination of Low-frequency Spectral Level, Ω_o

The effect of anelastic attenuation has not been considered in determining Ω_o from the Lg-wave amplitude spectrum at each station. It is well known that attenuation has an insignificant effect upon estimates of the spectral density within the low frequency band (f < 1 Hz) at which the Ω_o levels were set in most cases. The Lg-wave amplitude decrement due to the anelastic attenuation is proportional to $e^{-\gamma R}$, where R is epicentral distance and γ is coefficient of anelastic attenuation, which in its turn, is related to the quality factor Q by (Nuttli, 1986),

$$\gamma(f) = \pi f/U(f)Q(f)$$

where f is wave frequency and U is Lg-wave group velocity. The reported values of γ for 1 Hz Lg wave are 0.0006 km^{-1} for both central and southeastern United States (Nuttli, 1983; Bollinger, 1979), while Chun et al. (1987) reported $\gamma(f) = 0.0008\ f^{0.81}\ km^{-1}$ for eastern Canada.

Hence, according to the above results, by neglecting the effect of anelastic attenuation, we would introduce an error of a factor of about 3 at a distance of 1000 km for the 1 Hz spectral component. Since most of the observations in this study were made at distances significantly less than 1000 km, the attenuation correction becomes insignificant. Note that Ω_o is measured from the peak values of spectral densities at low-frequencies (see e.g., Figure 3-1). When Ω_o is measured from average values of the low-frequency level, then a multiplication factor of 2 is used to obtain the correct Ω_o (see Herrmann & Kijko, 1983).

3.1.4 Determination of Corner Frequency, f_o

Most of the deduced corner frequencies, f_R , were in the range from 1 to 5 Hz. Figure 3-2 depicts the observed corner frequencies as a function of epicentral distance. In agreement with the above reasoning, amplitudes of spectral components of frequencies greater than 1 Hz show significant decrement due to the attenuation, in particular, at large epicentral distances (cf. $e^{-\gamma R}$).

The correction for the effect of anelastic attenuation upon obtained corner frequencies is difficult, since the actual attenuation coefficient is not well known for Lg waves in the frequency range of interest (1 to 5 Hz). Further, it is not yet clear whether the attenuation due to scattering might be as important as the anelastic attenuation at this frequency band (e.g., Aki, 1980; Dainty, 1981).

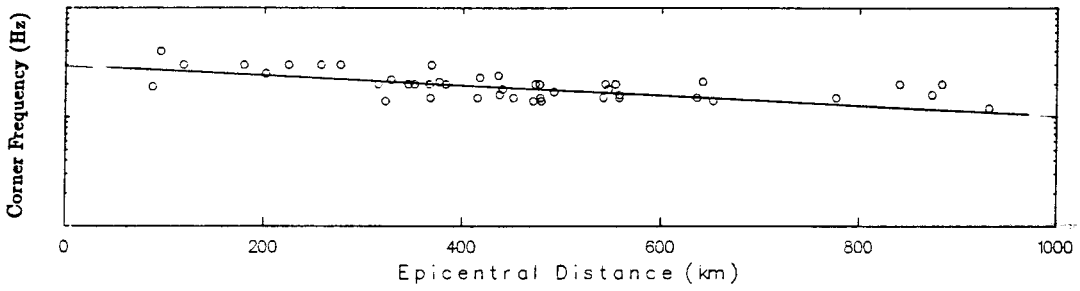

Figure 3-2. Observed corner frequencies plotted as a function of epicentral distance. Linear regression fit is indicated by a straight line.

On the other hand, it is realized that the epicentral distance is another important factor for the attenuation of the spectral components. It is observed that, in the first-order approximation, the measured corner frequencies of the Lg-wave spectra show remarkable linear dependence upon the epicentral distance (see Figure 3-2). Hasegawa (1983) reported similar findings for eastern Canada earthquakes.

The observed dependence of the corner frequency upon the epicentral distance was used to derive an empirical relationship between the observed corner frequency and epicentral distance. A linear regression line is fitted to the corner frequencies and the slope of the line is used to correct the observed corner frequency, f_R. The regression relation obtained is,

$$\log f_R = 0.45 - 0.00035\ R$$

The corrected corner frequencies deduced from records from different stations, are averaged to obtain a single corner frequency for each event. This frequency represents the source spectrum corner frequency, f_o, for any particular event.

3.2 Dynamic Source Parameters

3.2.1 Seismic Moment

Seismic moment, M_o, for the events studied is determined by making use of the low-frequency spectral level, Ω_o, through the relation derived empirically by Street et al. (1975) and verified theoretically by Herrmann & Kijko (1983),

$$M_o = \begin{cases} 4 \pi \rho \beta^3 R_o (R/R_o) \Omega_o & \text{for } R \leq R_o \\ 4 \pi \rho \beta^3 R_o (R/R_o)^{1/2} \Omega_o & \text{for } R > R_o \end{cases}$$

where ρ is density, β is shear wave velocity and R_o is the reference distance. For Fennoscandian shield earthquakes, values adopted in the above formula were ρ = 2.7 g/cm , β = 3.6 km/s and R_o = 100 km. R_o is used to account for different nature of Lg-wave geometrical spreading. That is, at near distance ($R \leq R_o$), spreading is typically like for body-waves (spherical), while it is like for surface waves (cylindrical) at greater distances ($R > R_o$).

The above moment formula is based on the relation between the seismic moment and the far-field low-frequency spectral level of the S wave (Keilis-Borok, 1960). Note that the radiation pattern correction for the far-field spectra is not considered here, since the Lg-wave train is composed of a family of rays which undergo subsequent multiple reflections and conversions as well as scattering within the crustal wave guide (see e.g., Campillo et al., 1984; Kim, 1987). This averages out the effect of the radiation pattern. The seismic moment for each event is obtained by averaging over all stations. Estimates of seismic moments for the events studied are listed in Table 3-1.

Table 3-1 Source Parameters of Earthquakes in northern Sweden

Event no.	Date	Origin time (h m s)	Seismic moment (dyne-cm)	Magnitude M_L
1	4 Jan. 1967	04 44 17	1.6×10^{20}	3.2
2	13 Apr. 1967	08 46 15	5.3×10^{20}	3.7
3	4 Sept.1968	17 09 15	4.2×10^{20}	3.4
4	4 Jul. 1969	22 28 54	2.0×10^{20}	3.1
5	17 Apr. 1971	08 05 01	1.0×10^{20}	3.1
6	17 Apr. 1973	06 17 55	2.8×10^{20}	3.3
7	1 Dec. 1974	19 35 56	1.1×10^{20}	3.2
8	11 Aug. 1975	18 28 10	1.1×10^{21}	3.9
9	16 Jan. 1978	02 28 24	1.6×10^{20}	3.2
10	28 May 1980	10 36 45	1.2×10^{20}	3.1
11	31 Jan. 1982	03 38 54	1.8×10^{20}	3.1
12	4 Jan. 1983	20 51 04	3.0×10^{20}	3.4
13	25 Aug. 1984	19 39 14	1.0×10^{20}	3.1
14	2 Apr. 1985	19 29 40	1.5×10^{20}	3.2

3.2.2 Source Radius and Stress Drop

By assuming a circular fault model, the source radius, r, is estimated by using the corrected source spectrum corner frequency, f_o, through the relation (Brune, 1970 & 1971),

$$r = 2.34 \beta / 2\pi f_o$$

The calculated source radii range from 0.4 to 0.6 km and are listed in Table 3-2. Note that the source radii for all the events are nearly constant.

The stress drop, $\Delta\sigma$, is estimated by using the above fault radius and the seismic moment through the formula (Keilis-Borok, 1959; Kanamori & Anderson, 1975),

$$\Delta\sigma = (7/16)\, M_o / r^3$$

Estimates of stress drops fell between 0.3 and 5.3 bars. The stress drops for the events studied are listed in Table 3-2.

Table 3-2 Source Parameters of Earthquakes in northern Sweden

Event no.	Date	Origin time (h m s)	Source radius r (km)	Stress drop $\Delta\sigma$ (bars)
1	4 Jan. 1967	04 44 17	0.47	0.69
2	13 Apr. 1967	08 46 15	0.47	2.19
3	4 Sept.1968	17 09 15	0.46	1.92
4	4 Jul. 1969	22 28 54	0.41	1.27
5	17 Apr. 1971	08 05 01	0.47	0.42
6	17 Apr. 1973	06 17 55	0.54	0.77
7	1 Dec. 1974	19 35 56	0.56	0.29
8	11 Aug. 1975	18 28 10	0.45	5.31
9	16 Jan. 1978	02 28 24	0.48	0.63
10	28 May 1980	10 36 45	0.47	0.52
11	31 Jan. 1982	03 38 54	0.50	0.64
12	4 Jan. 1983	20 51 04	0.45	1.46
13	25 Aug. 1984	19 39 14	0.46	0.48
14	2 Apr. 1985	19 29 40	0.50	0.53

As follows from Table 3-2, stress drops of the events studied are small compared with those of other regions. For example, stress drops obtained by Bungum et al. (1982) for the Meloy earthquake sequence in northern Norway (seismic moment range from 10^{17} to 2 x 10^{19} dyne-cm) as well as those for the events in southern Sweden studied by Slunga et al. (1984, see their figure 6, moment range from 10^{18} to 10^{2} dyne-cm) reveal an order of magnitude larger stress drops compared with our results for the events with comparable size.

Although, Brune et al. (1986) suggested a possible existence of small, low-stress drop events (partial stress drop model of Brune, 1970) intermixed with high-stress drop events in a given source region, it is difficult to explain such a large discrepancy. It might be partly due to errors in determining the correct corner frequencies from regionally recorded Lg waves, since, the effect of wave propagation path (e.g., anelastic attenuation) could not be fully accounted for due to rather complex Lg wave propagation paths.

The source radii for the 14 northern Sweden earthquakes obtained from the corner frequencies are nearly constant over the seismic moment range from 10^{20} to 10^{21} dyne-cm. Although, there are some uncertainties in the measured corner frequencies mainly due to low quality analog data used, this constancy leads to a strong dependence of stress drop on seismic moment. The earthquakes studied are characterized by a steadily increasing stress drop relative to increasing seismic moment, which is a consequence of the observation that the corner frequency decreases with increasing moment by the slope greater than -3. A slope of -3 would imply a constant stress drop (Brune, 1970).

4. WAVEFORM MODELING AND SOURCE MECHANISM

In this section, we discuss characteristics of observed seismograms from earthquakes in northern Sweden and the method to calculate corresponding synthetic seismograms. The focal depths and source mechanisms of the earthquakes are constrained by a trial-and-error fit of the synthetic seismograms to the observations.

4.1 Observational Data

The events studied occurred in northern Sweden and are typical small regional earthquakes. These events are usually recorded by only a few short-period seismographs at regional distances (Δ = 100 - 1000 km). Thus, for these earthquakes, it is difficult to determine reliably their focal depths and source mechanisms, due to the paucity of high-quality data as well as to the difficulties in interpreting the regional short-period records. Observed seismograms from nearby earthquakes (Δ < 100 km) often exhibit relatively simple waveforms and the P and S waves are easy to discern. As the epicentral distance increases, the observed seismograms become more complex and the characteristic crustal phases, such as Pn, Pg, Sn and Lg phases, are observed at regional distances. These phases often consist of successive arrivals distributed over intervals from a few seconds to a few tens of seconds (see e.g., Campillo et al., 1984; Kim, 1987).

The regional records analysed consist mainly of three-component short-period seismograms and are the same as those described in Section 3. The epicentral distance range of the stations used is between 50 and 500 km. Seismograms recorded at epicentral distances greater than about 500 km show crustal phases that are too weak to be analyzed. N-S and E-W components pair of seismogram are rotated into its back azimuth to obtain radial and transverse components. Below, we discuss briefly characteristics of records from the two largest events, i.e., from the events on 11 August 1975 and on 13 April 1967. Other smaller events exhibit similar observations but usually provide a lower number of records.

Event on 11 August 1975:

This event is the strongest event which have occurred in the region during the last 25 years. It has a seismic moment of 1.1×10^{21} dyne-cm and magnitude of M_L = 3.9. Figure 4-1a shows the vertical-component short-period seismogram sections from this event made at seismograph stations UME, KEV and KJF by Benioff seismographs and at the station KIR equipped with a Grenet-Coulomb seismograph. The corresponding radial and transverse components are shown in Figure 4-1b and 4-1c, respectively.

A quick glance at Figure 4-1 reveals that Lg waves consist of several successive arrivals and extend over about 20 s on all three components. Sn phase has substantial energy on all three components at UME, whereas Pg phase is clearly visible on all three components of seismograms from KJF. At all stations, Lg wave arrives with a group velocity of between 3.6 and 3.7 km/s.

Event on 13 April 1967:

This event is the second largest event among the events studied. It has a magnitude of M_L = 3.7 and a seismic moment of 5.3×10^{20} dyne-cm. Figure 4-2a shows the vertical-component seismogram sections from this event. The corresponding radial and transverse components are shown in Figure 4-2b and 4-2c, respectively. As shown in the figure, overall characteristics of the observed waveforms are similar to those of the event on 11 August 1975. Nevertheless, there are some differences. For example, on the seismogram trace from UME, the Lg wave consists of fewer pulses and appears to be shorter in duration and simpler in appearance.

4.1.1 Band-Pass Filtering of Data

The digitized short-period data comprise high-frequency noise introduced during the manual digitizing process. There also is a low-frequency noise present in the data due to the earth's ambient background noise.

To reduce the influence of both types of noise and other unnecessary complications in the data, a band-pass third-order Butterworth filter with low- and high-cutoff frequencies of 0.5 and 1.6 Hz, respectively is applied to the observed traces. This procedure also eliminates much of the unnecessary noises, mainly due to local earth's structure, in the data.

Filtered vertical-component seismogram sections are shown in Figures 4-3a and 4-3b which correspond to unfiltered observed data shown in Figures 4-1 and 4-2, respectively. As shown in the figure, the filtered traces preserve overall characteristics of phases on the original traces, especially their polarities and waveforms. The low- and high-frequency noise of the original traces is minimized on filtered records. Throughout this study, the band-pass filtering is applied to both the observed and synthetic traces for consistent comparisons.

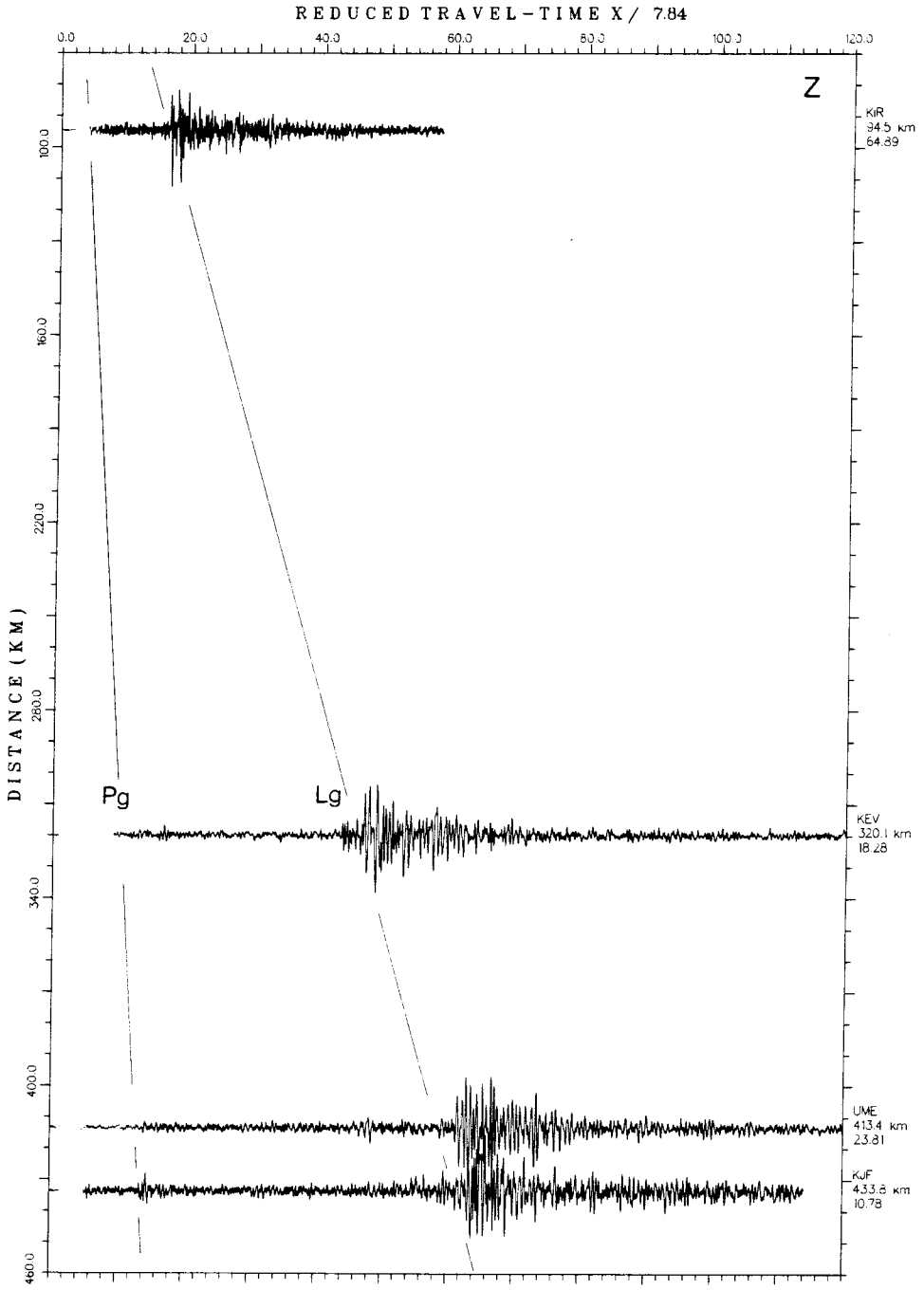

Figure 4-1a. Short-period vertical-component (Z) seismogram sections from the event on 11 Aug. 1975. Seismogram traces are plotted with a reduction velocity of 7.84 km/s and each trace is normalized to the maximum trace amplitude. Trace peak-to-peak amplitude (in millimeters) is shown at the end of each trace. The straight lines indicate group velocities of 4.6 km/s and 3.6 km/s corresponding to Pg and Lg wave arrivals, respectively.

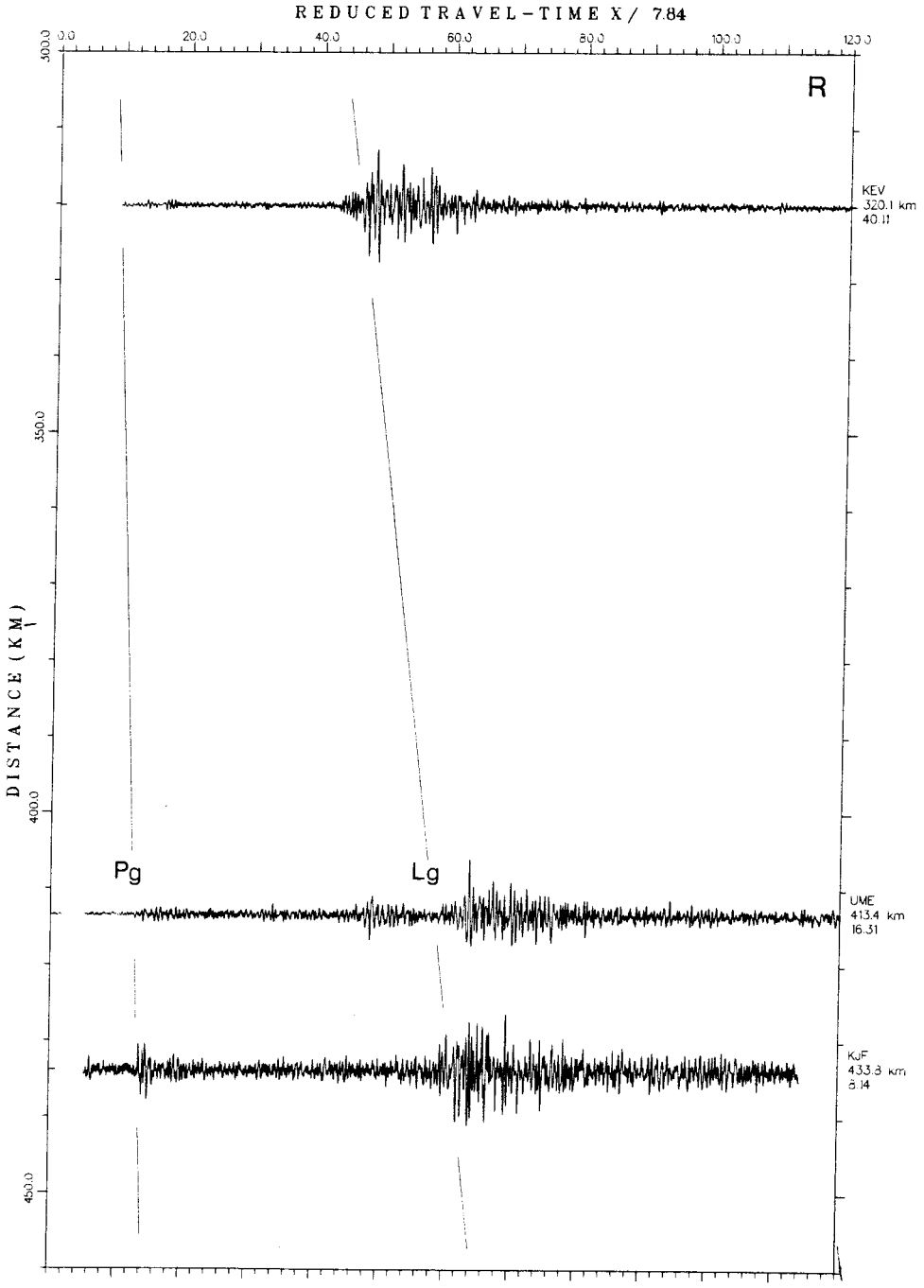

Figure 4-1b. Rotated short-period radial-component (R) seismogram sections from the event on 11 Aug. 1975. Other notations are the same as in Figure 4-1a.

21

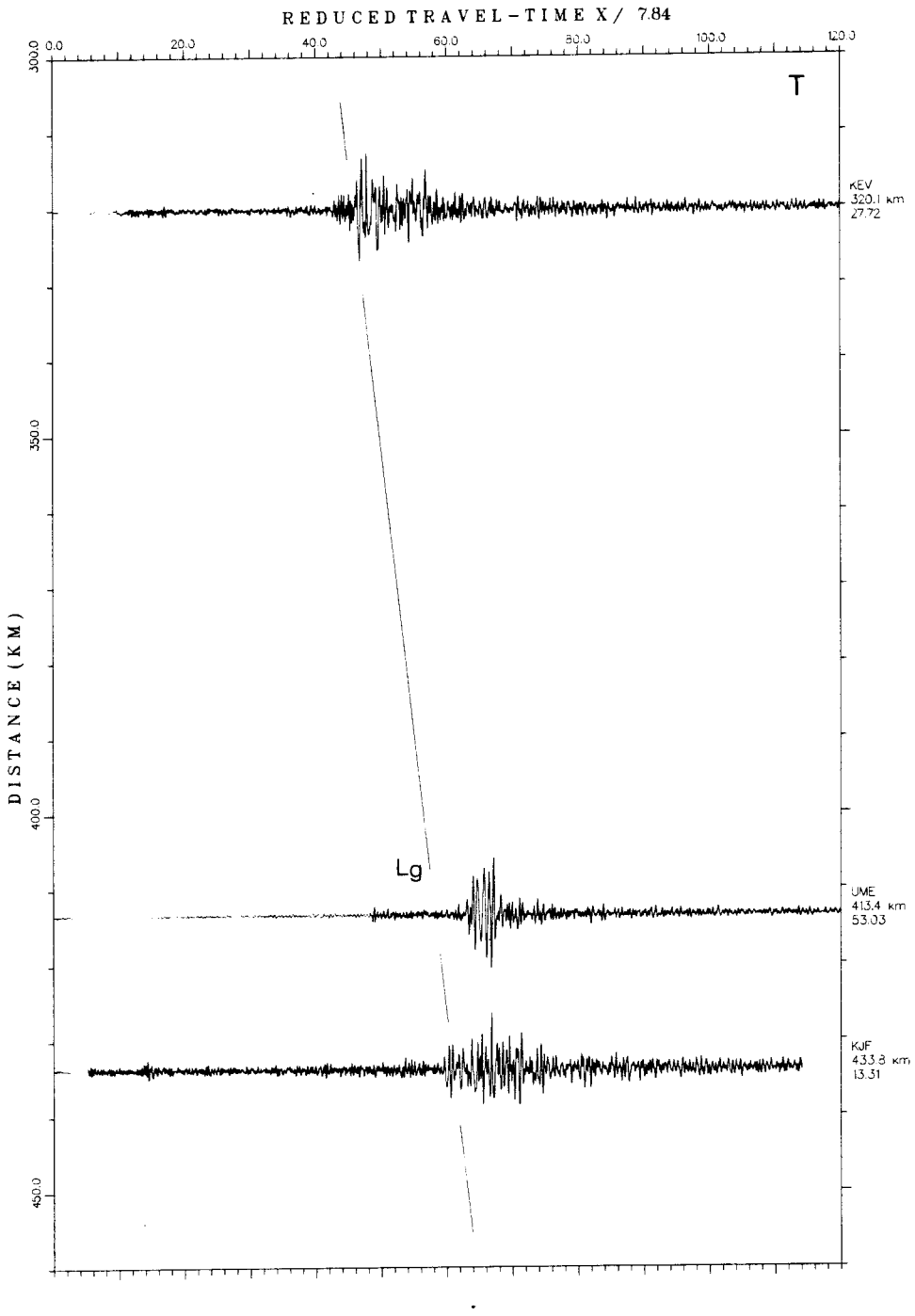

Figure 4-1c. Rotated short-period transverse-component (T) seismogram sections from the event on 11 Aug. 1975. Other notations used are the same as in Figure 4-1a.

22

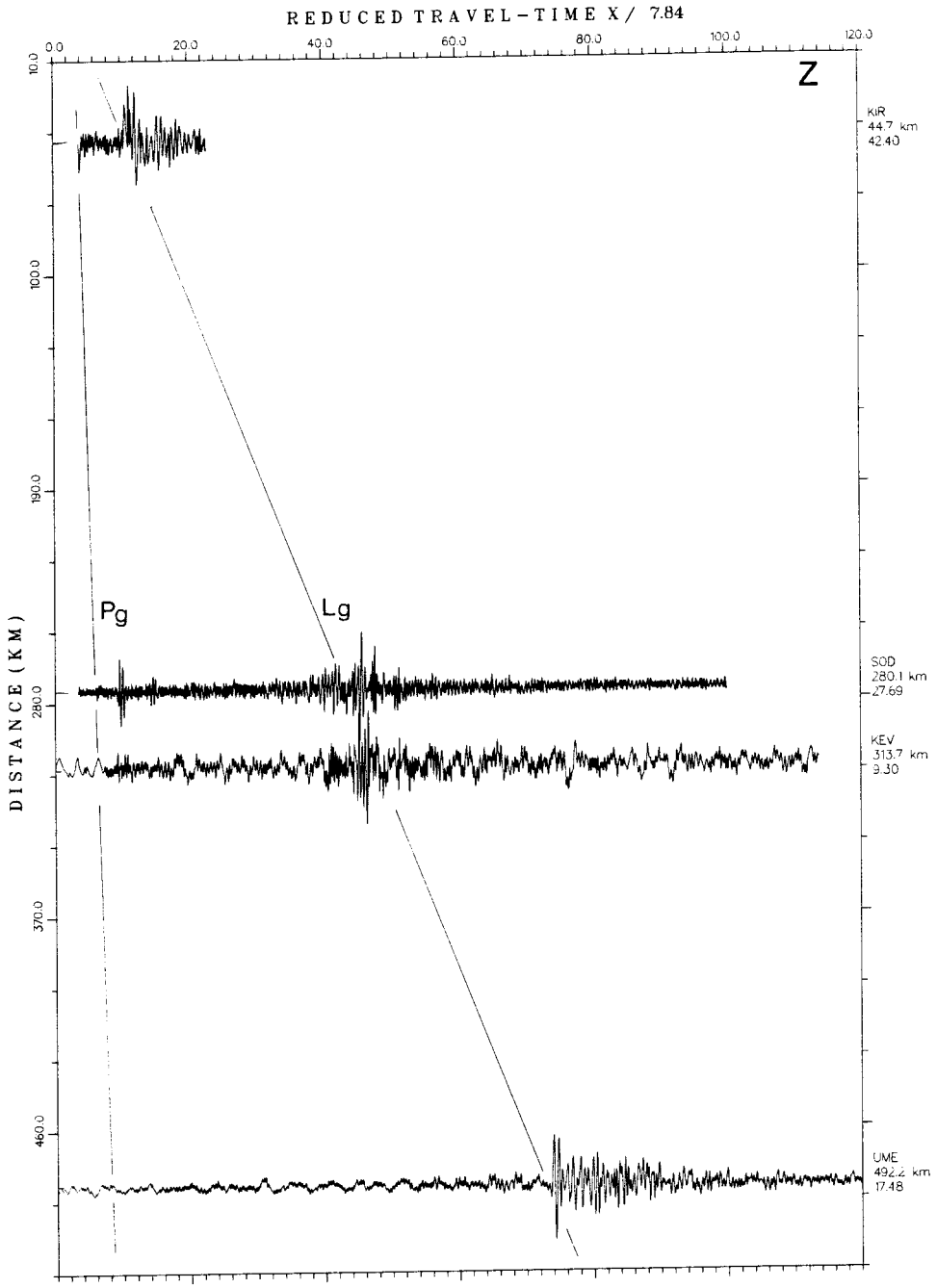

Figure 4-2a. Short-period vertical-component (Z) seismogram sections from the event on 13 Apr. 1967. Seismogram traces are plotted with a reduction velocity of 7.84 km/s and each trace is normalized to the maximum trace amplitude. Trace peak-to-peak amplitude (in millimeters) is shown at the end of each trace. The straight lines indicate group velocities of 4.6 km/s and 3.6 km/s corresponding to Pg and Lg wave arrivals, respectively.

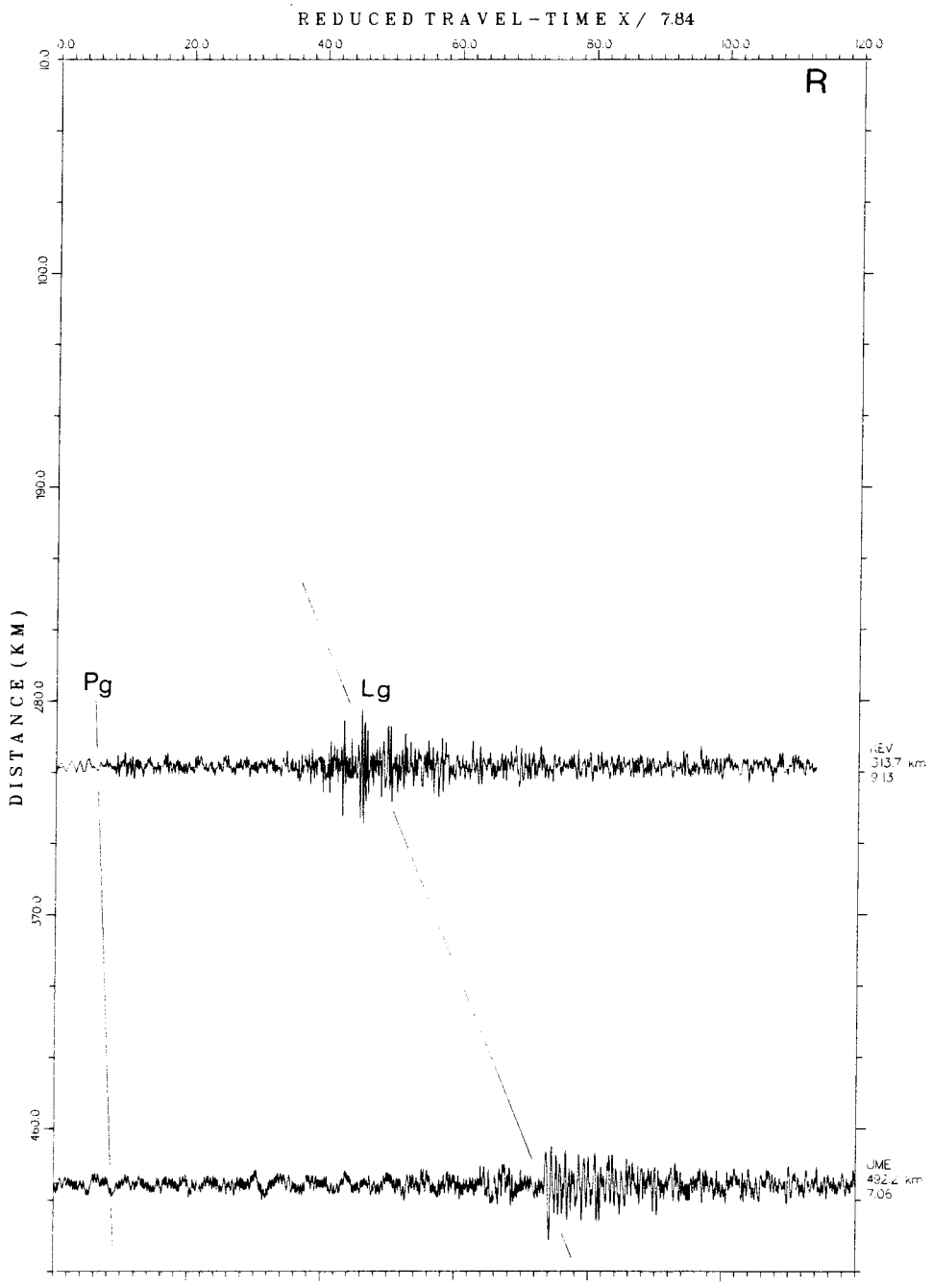

Figure 4-2b. Rotated short-period radial-component (R) seismogram sections from the event on 13 Apr. 1967. Other notations are the same as in Figure 4-2a.

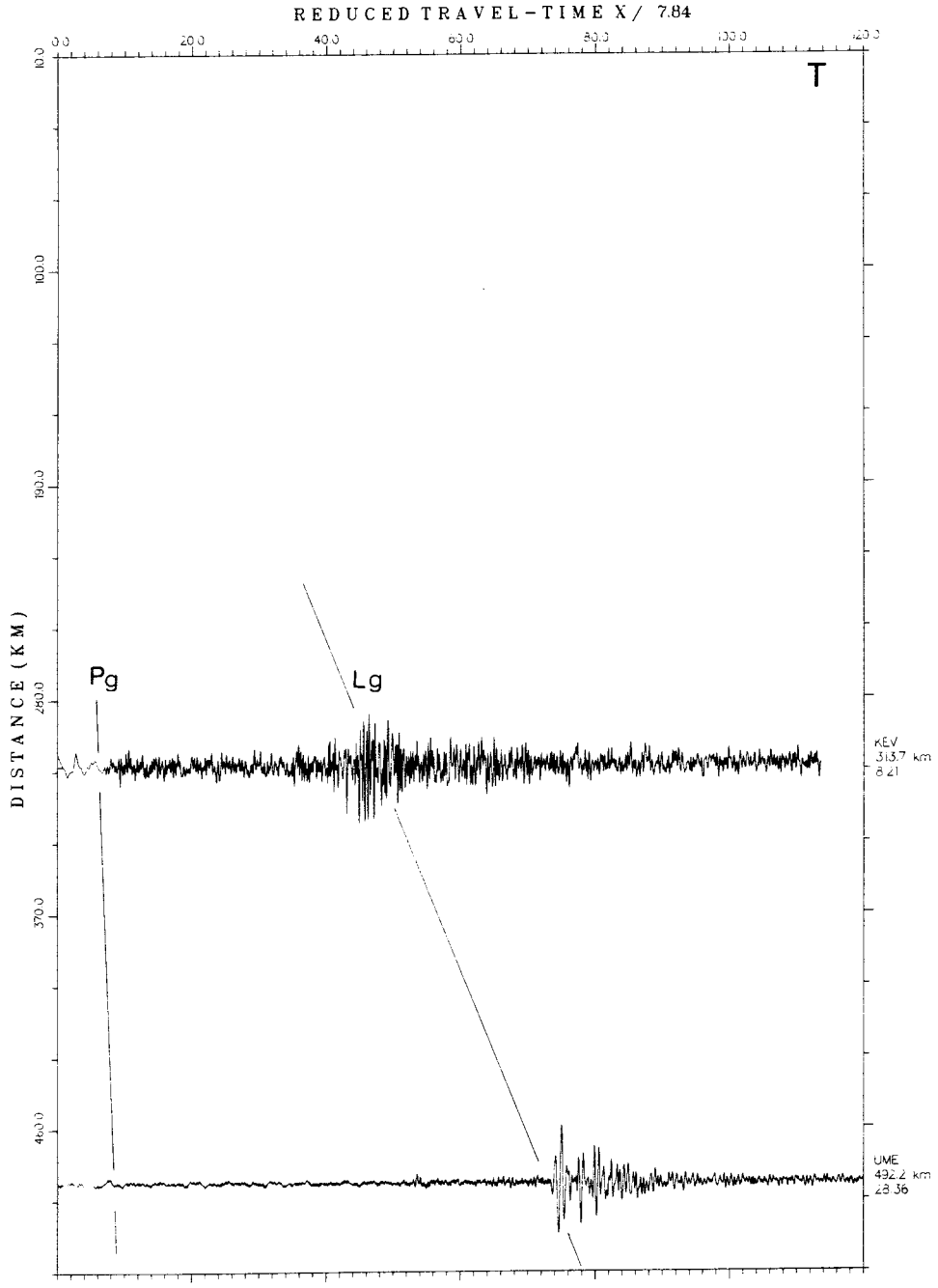

Figure 4-2c. Rotated short-period transverse-component (T) seismogram sections from the event on 13 Apr. 1967. Other notations are the same as in Figure 4-2a.

4.2 Synthetic Seismograms

To constrain focal depths and source mechanisms of the studied earthquakes, we employed complete synthetic seismograms calculated for a point shear-dislocation source embedded in a layered crustal structure. The complete synthetic seismograms for the regional events are computed by using the discrete wavenumber summation method (Buchon, 1981).

The crust velocity model for Sweden (Båth, 1979) is used for all stations and a moderate level of anelastic attenuation is included in the calculation using the attenuation factor, Q, for both P and S waves. The model consists of an upper crust with thickness of 19 km and a 19 km thick lower crust. The upper crust is characterized by the P-wave velocity of 6.22 km/s and S-wave velocity of 3.58 km/s, whereas the lower crust has the P- and S-wave velocity of 6.44 km/s and 3.69 km/s, respectively. The P- and S-wave velocity across the crust-mantle boundary at a depth of 38 km jump to 7.84 km/s and 4.55 km/s, respectively. The crust model used is listed in Table 4-1.

Table 4-1 Seismic Velocity Model for Northern Sweden.

Thickness (km)	V_P (km/s)	V_S (km/s)	Density (g/cm^3)	Q_P	Q_S
19	6.22	3.58	2.7	1200	800
19	6.64	3.69	2.9	1500	1000
uppermost mantle	7.84	4.55	3.1	2000	1500

The quality factor, Q, for the anelastic attenuation assigned to each layer is somewhat arbitrary. However, it is based on recent findings that the Q factor for the S wave at a frequency of 1 Hz ranges from about 900 to 1100 in the crust and that the Q factor depends upon the frequency as

$$Q(f) = Q_o f^{\eta} \quad \text{for } 0.6 \leq f \leq 10 \text{ Hz}$$

where f is frequency, Q_o is P or S wave Q factor at 1 Hz and η is a numerical constant. In the case of eastern Canada, Q_o for S wave ranges from 900 to 1100 and η is about 0.2 (see

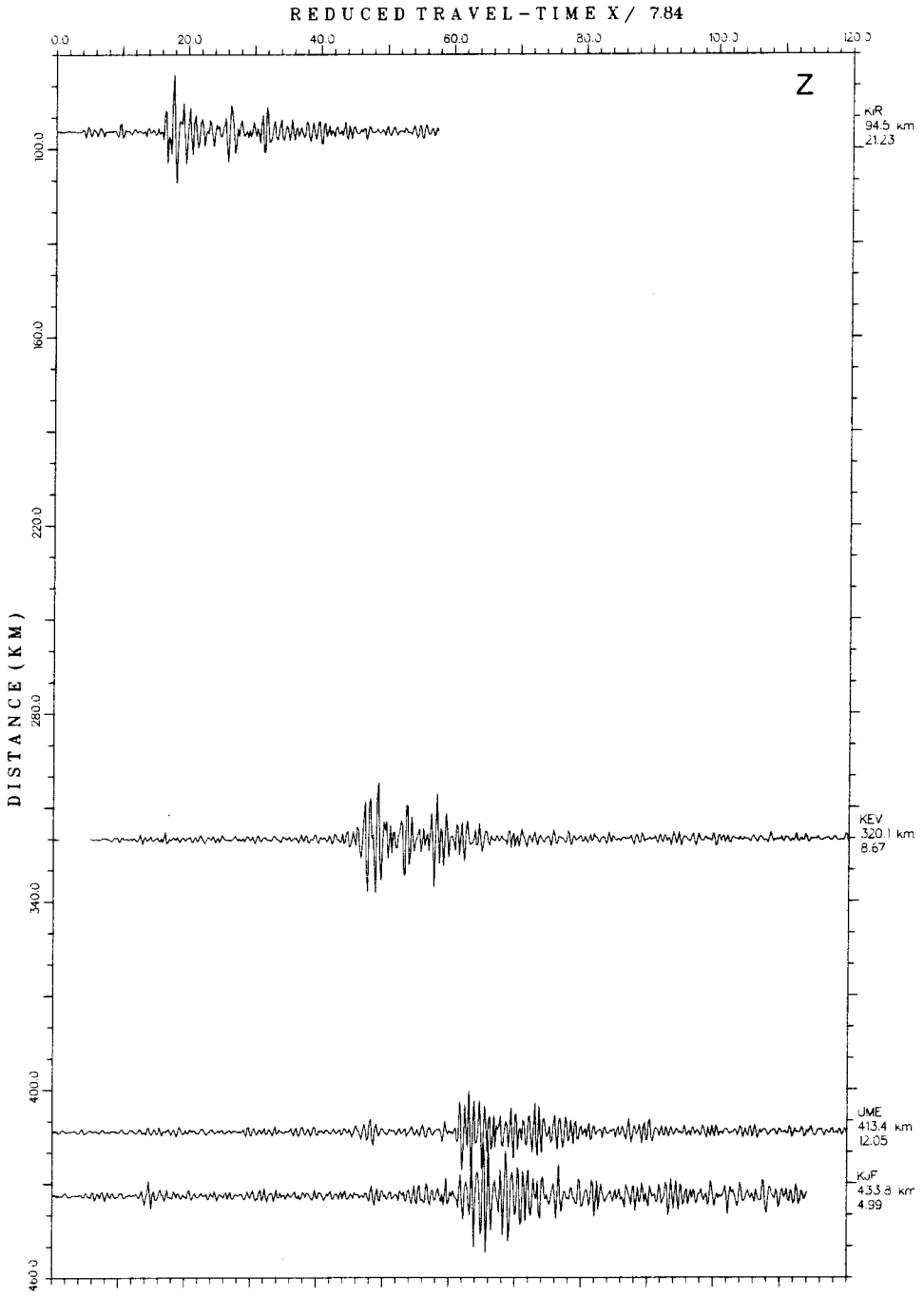

Figure 4-3a. Band-pass filtered seismograms corresponding to the observed short-period vertical-component (Z) seismogram sections from the event on 11 Aug. 1975 shown in Figure 4-1a. Other notations are the same as in Figure 4-1a.

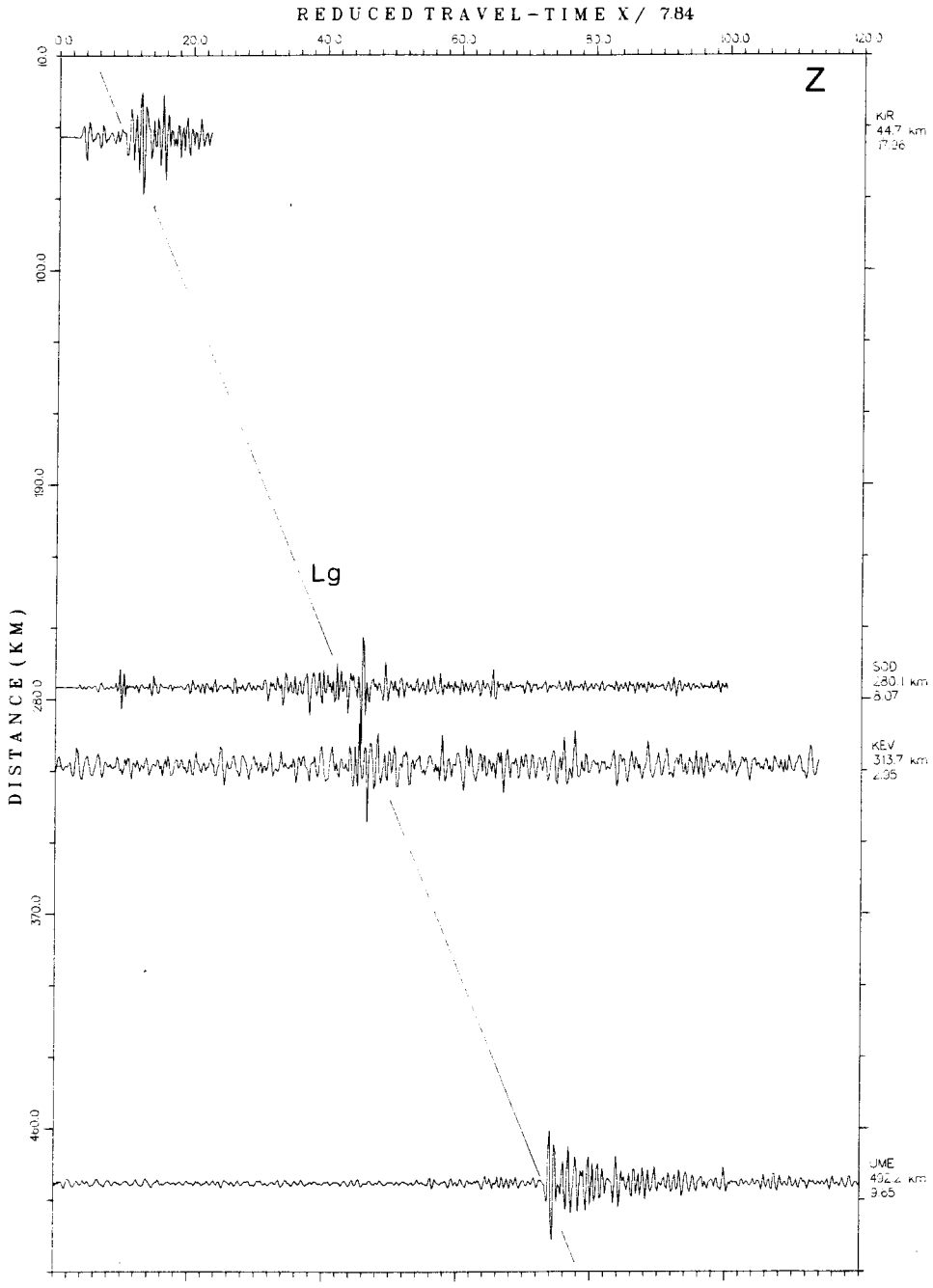

Figure 4-3b. Band-pass filtered seismograms corresponding to the observed short-period vertical-component (Z) seismogram sections from the event on 13 Apr. 1967 shown in Figure 4-2a. Other notations are the same as in Figure 4-2a.

Hasegawa, 1985; Chun et al., 1987). For Sweden, Slunga (personal communication) suggests Q_o=480 and η =0.5 for S waves. These results provide a Q for the S wave between 1070 and 1370 at a frequency of 5 Hz.

We choose Q_o=800 for the S wave in the upper crust, whereas Q_o=1000 is assigned for the lower crust. In this case, the Q factor for the S wave at 5 Hz becomes 1103 and 1380 for the upper and lower crust, respectively. Thus, our choice of Q_o's is consistent with above findings and seems to be reasonable. The Q factor for the P wave is chosen to be of about a factor of 1.5 larger than that for the S wave (see Table 4-1).

The source time function used for the synthetic seismogram calculations is assumed to be known. The spectral analysis of vertical-component Lg waves recorded at seismograph stations in Sweden and Finland suggested that all the events had the source radii of about 0.45 to 0.6 km (see Section 3). Assuming a rupture velocity of about 2.7 km/s (approx. 0.75β), the total rupture duration is about 0.2 s. Thus, a ramp type source time function with rise time of about 0.2 s was used to compute the synthetics. The synthetic seismograms are calculated for the ground displacement convolved with source time function and the Benioff short-period seismograph response.

4.2.1 Effect of Anelastic Attenuation

As discussed in Section 3, the anelastic attenuation in the crust is not well known for northern Sweden. In order to assess the effects of anelatic attenuation on the calculated synthetic seismograms, we constructed synthetics for two different attenuation models for the sake of comparison.

The first set of synthetics, calculated for the crust Q model listed in Table 4-1, is shown in Figure 4-4 (lower traces). For the second set of synthetics, we used somewhat lower Q values, that is, higher level of attenuation in each layer. The upper crust has Q_S of 300 and Q_P of 500, whereas Q_S=400 and Q_P=1000 are assigned for the lower crust. At the top of the upper mantle, just beneath the Moho, Q_S and Q_P increase to 900 and 1500, respectively. The synthetics for the latter model are also shown in Figure 4-4 (upper traces).

Results of computations for the high and low Q crust models used are shown in Figure 4-4. As follows from the figure, there is very little difference in amplitudes and waveforms between the two traces at short epicentral distance (see traces for KIR). However, as the epicentral distance increases, the amplitudes of the early arrival portion of Lg waves calculated for the high Q model increase gradually compared with those for the low Q model. At epicentral distances greater than 300 km, the amplitudes of Lg waves on the synthetics for the high Q model are greater than those for the low Q model by a factor of 2. Note that there are much less variations in the P-wave amplitudes between the traces for the two Q models.

Another set of synthetics is calculated by incorporating a frequency dependent Q factor for both the P and S waves. In the calculation, we allow Q vary with frequency, for frequencies higher than 1 Hz, as $Q(f) = Q_0 f^{\eta}$. The results of the computation are very similar to those of the first set of synthetics shown in Figure 4-4.

The synthetics calculated for the low and high Q crust models indicate that the waveforms of the crustal phases, especially the Lg waves, are not so sensitive for a reasonable variation in the crustal Q models. However, the amplitude of Lg waves varies significantly depending upon the Q model used. That is, the high Q model produces higher Lg-wave amplitudes than the low Q model and the amplitude difference between the two models increases with increasing epicentral distance.

4.3 Source Mechanisms

The standard method of obtaining the earthquake source mechanism by employing the stereographic projection of P-wave first motions could not be used for the small earthquakes in northern Sweden. Most of the events provide only a few records due to the small event size and to few seismograph stations operating around the epicentral region. With only a few exceptions, even for those few available seismograms, it is difficult to determine the P-wave first motion polarities with confidence, since most of the observed first arrivals are very weak.

In the present study, we used the entire seismic wave train of the observed records and compared them with complete synthetic seismograms calculated for the regional distances to constrain the source mechanisms. Waveform inversion method could not be applied, since it was impossible to synchronize major phases on both the observed and synthetic records for these small earthquakes, due to the uncertain source location as well as to the effect of unknown crustal structure along the wave propagation paths. The records also showed too weak phases with strong background noise.

Therefore, the synthetic waveforms are matched to the observed records by a trial-and-error fit. Criteria to search for the best fit synthetics for the source mechanism parameters were the following:

- relative amplitudes of P- and Lg-wave trains,
- agreement between observed and synthetic Lg waveforms,
- amplitude ratios between the synthetic and observed records for all the stations,
- observed P-wave first motion polarities.

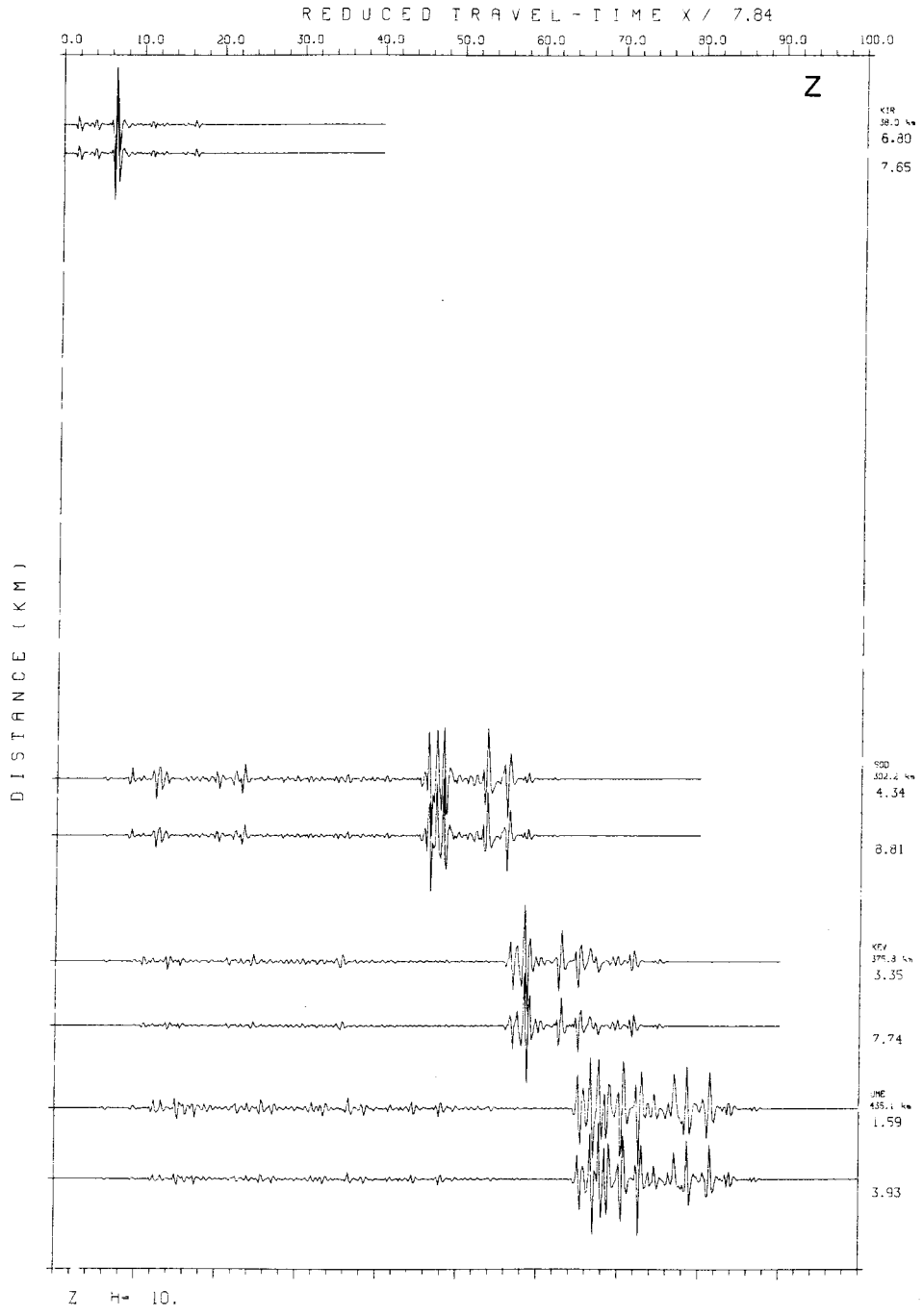

Figure 4-4. Vertical-component synthetic seismograms calculated for a vertical dip-slip event embedded in crust models with different Q values. The upper trace at each station is for a crust model with high Q values and the lower trace is for a low Q crust model.

In the following, we discuss the waveform modeling for the two largest earthquakes and show the final best fit synthetics for the two events.

Event on 11 August 1975

The first step in the waveform modeling procedure was to constrain the focal depth for the event. A set of synthetic seismograms is calculated for various focal depths and compared with the observed records. The best fit synthetics are the ones which satisfy the relative arrival times between P and S waves as well as the separation between successive pulses in the Lg-wave train (see Figure 4-1). The best fit synthetic seismograms constrained the hypocenter to be at the upper crust at a depth of 12 km.

In the next step, we constrained the source mechanism parameters, such as strike, dip and slip angles. For this event, a clear P-wave first motions are observed at four stations, namely at KIR, SOD, MA and OUL. All clear polarity observations showed positive first motion. Though, the observed polarity data covered only the SE quadrant of the focal sphere, these first motion polarities were used to constrain the preliminary focal mechanisms (see Figure 4-5).

All three components of synthetic seismograms were calculated by employing known source mechanism parameters and compared with the observed records. In matching the synthetics to observations, we required that they are consistent also with observed P-wave first motion polarities and emphasis was put on the Lg wave portion of records.

The best fit synthetic seismograms constrain the orientation of nodal planes. The first nodal plane is a near-vertical plane (dip = 85^{o}) which has a strike = 350^{o} and a slip = 270^{o}. The second nodal plane is a shallowly dipping plane (see Figure 4-5). The first nodal plane represents a normal faulting on a near-vertical plane. Note that the strike of the first nodal plane is almost parallel to the direction (i.e., almost N-S) of the epicenter distribution in the eastern part of the source region (see Section 2).

A comparison of the vertical-component observed records and the final synthetic seismograms computed for the source mechanism parameters determined is shown in Figure 4-6a. As follows from the figure, the overall agreement of relative amplitudes and waveforms of the major phases between the observed and synthetic traces is fairly good, suggesting that the source

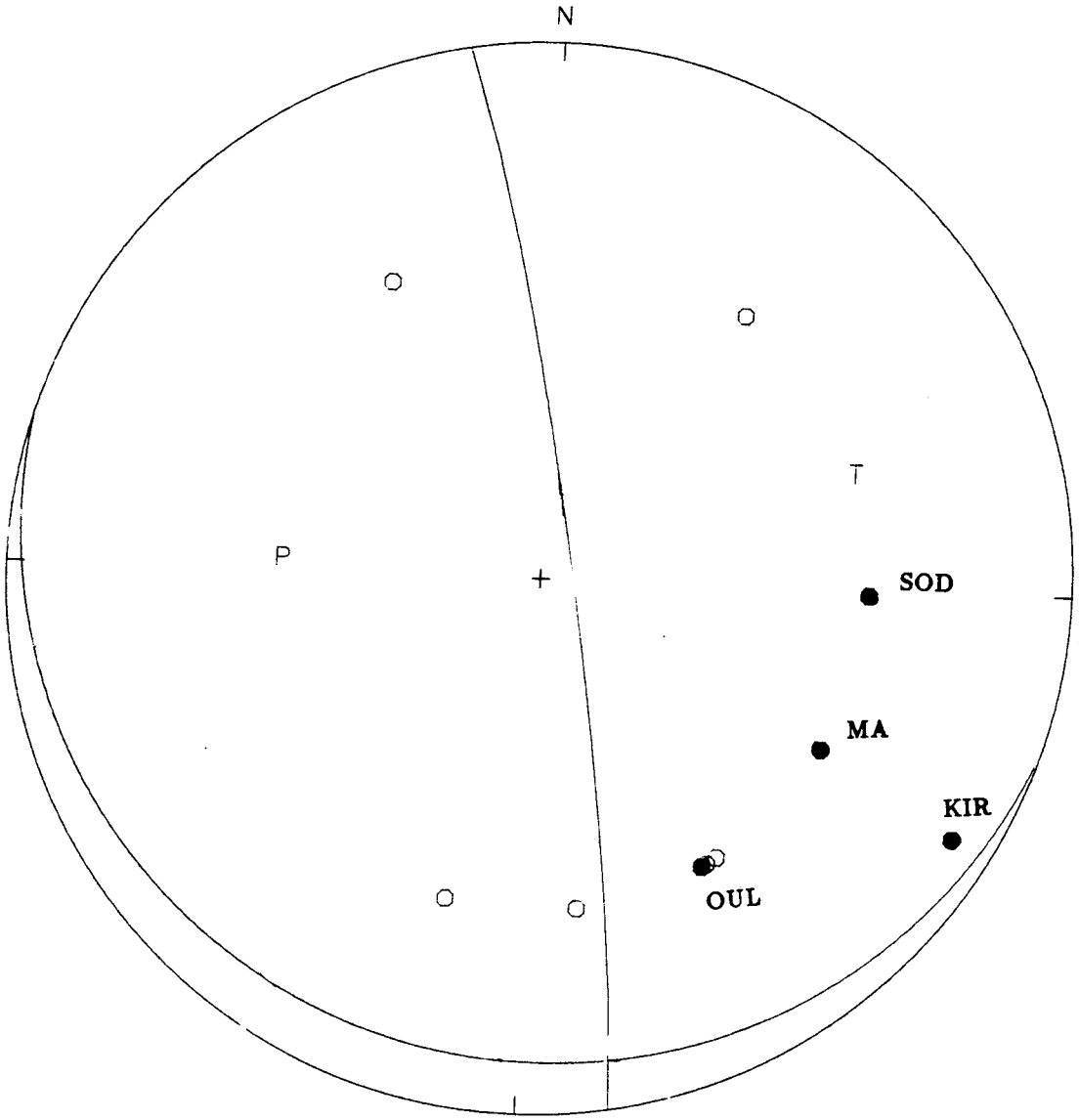

Figure 4-5. Focal mechanism for the event on 11 Aug. 1975. Nodal planes and pressure (P) and tension (T) axes are shown on an equal-area lower-hemisphere projection. Observed P-wave first motions are plotted with open circles and solid circles indicate clear positive first motions.

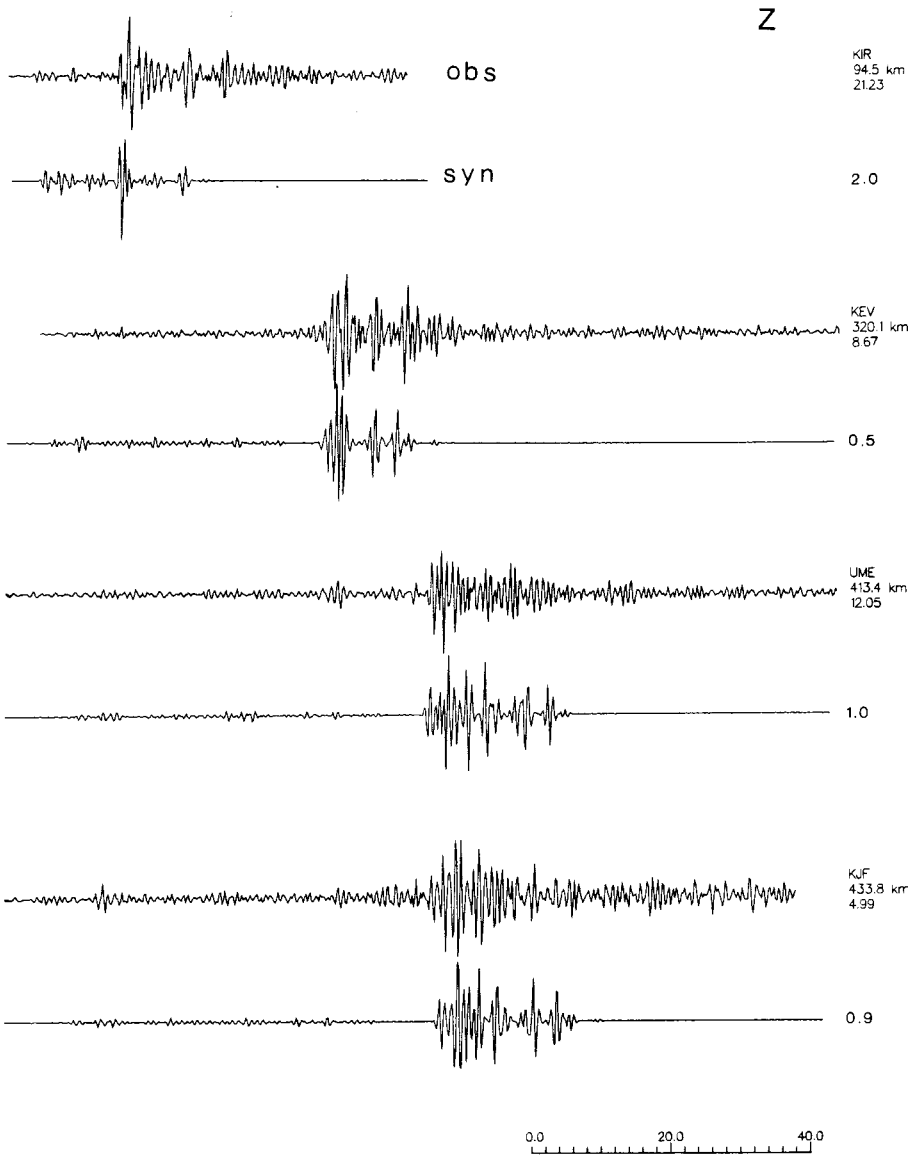

Figure 4-6a. Comparison of observed vertical-component records (upper traces) from the event on 11 Aug. 1975 with synthetic seismograms (lower traces). The numbers at the end of the synthetic traces indicate the ratio of the maximum amplitude of the synthetic trace to that of the observed trace. Note that the ramp type source time function with rise time of 0.2 s is used.

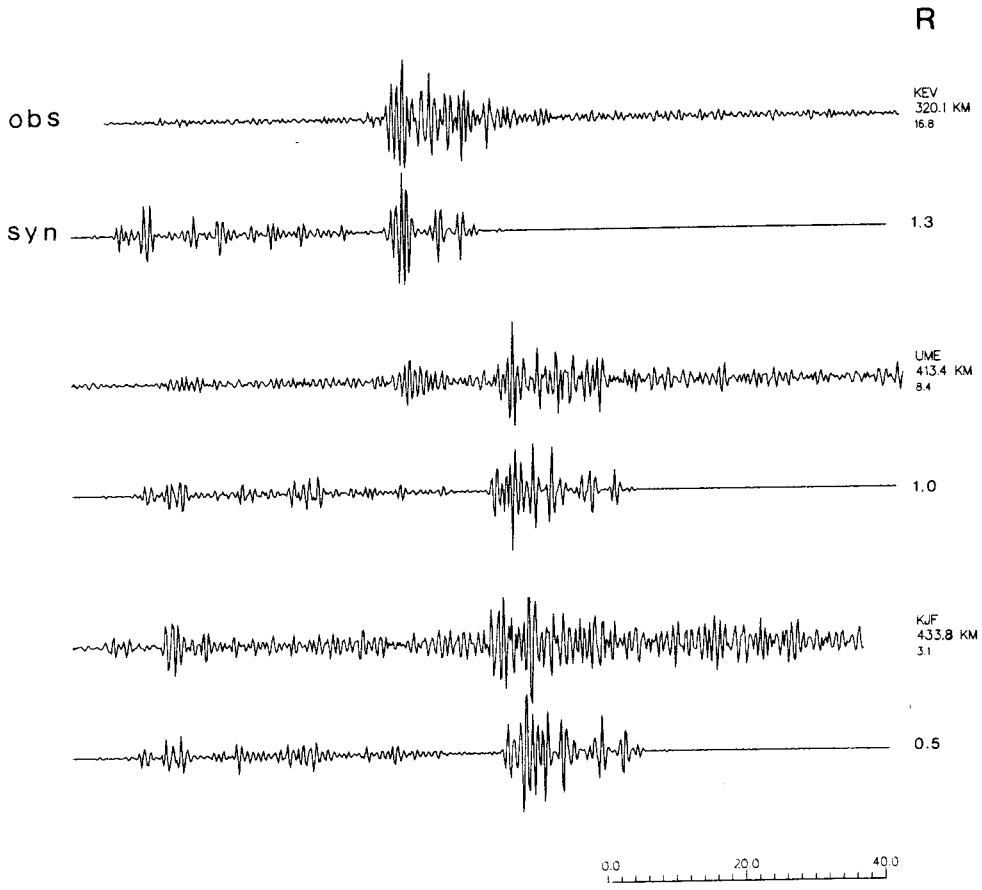

Figure 4-6b. Comparison of observed radial-component records (upper traces) from the event on 11 Aug. 1975 with synthetic seismograms (lower traces). Notations are the same as those in Figure 4-6a.

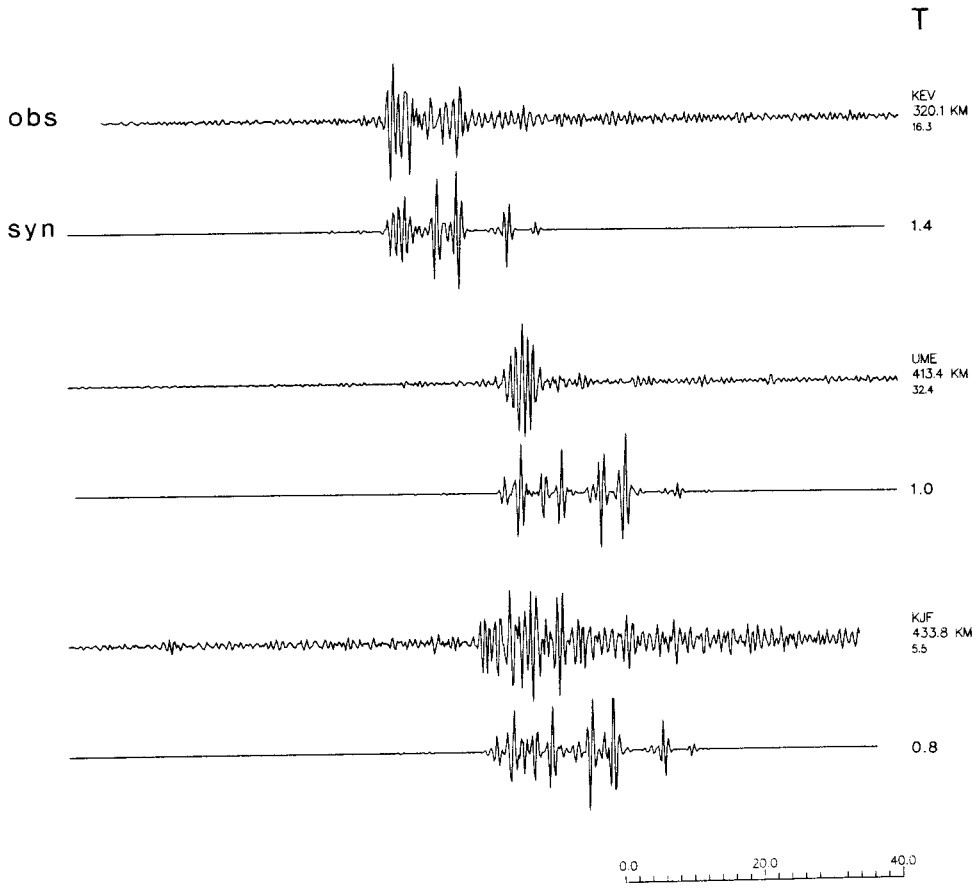

Figure 4-6c. Comparison of observed transverse-component records (upper traces) from the event on 11 Aug. 1975 with synthetic seismograms (lower traces). Notations are the same as those in Figure 4-6a.

mechanism and focal depth estimates are reasonable. Despite the overall satisfactory match, there are some discrepancies between the observations and synthetics. At station KEV, the observed amplitude is smaller than the synthetic by a factor of two, whereas the opposite is true for the station KIR.

Figures 4-6b and 4-6c exhibit the observed and synthetic radial and transverse components, respectively. These synthetic traces were computed with the same parameters as those used for the vertical component synthetics. In the case of the transverse component, the overall agreement between the observed and synthetic traces is rather poor and only the arrival times of the prominent phases are matched (see Figure 4-6c). The relative amplitude between the prominent phases on the observed traces are not very well reproduced by the synthetics. This feature is probably caused by the imperfect crustal model used to generate the synthetic traces.

The source mechanism parameters determined may not be unique and they may involve certain errors. Nevertheless, the orientation of the tension and pressure axes acting around the hypocenter of the event is reliable, since they are not sensitive to the small errors in the orientation of the two nodal planes. The pressure axes is trending due west and has a plunge angle of 50^{o} NW, whereas the tension axis is trending NE and its plunge is 40^{o} NE.

Event on 13 April 1967

The waveform modeling for this event followed the same procedure as that used for the previous event. The best fit synthetic seismograms placed the hypocenter of the event in the upper crust at a depth of 15 km.

For this event, clear positive P-wave first motions are observed at stations, KIR and OUL, wheras at stations SOD and TRO, the observed polarities were negative. Azimuthal coverage of the polarity data improved somewhat as they covered eastern half of the focal sphere. Observed polarities at KIR, OUL and SOD support the proposed orientation of nodal planes, while TRO does not.

The best fit synthetic seismograms constrained the orientation of nodal planes. The first nodal plane is a near-vertical plane (dip = 85^{o}) which has a strike = 260^{o} and a slip = 270^{o}. The second nodal plane is a shallowly dipping plane (see Figure 4-7). The first nodal plane represents a normal faulting on a near-vertical plane.

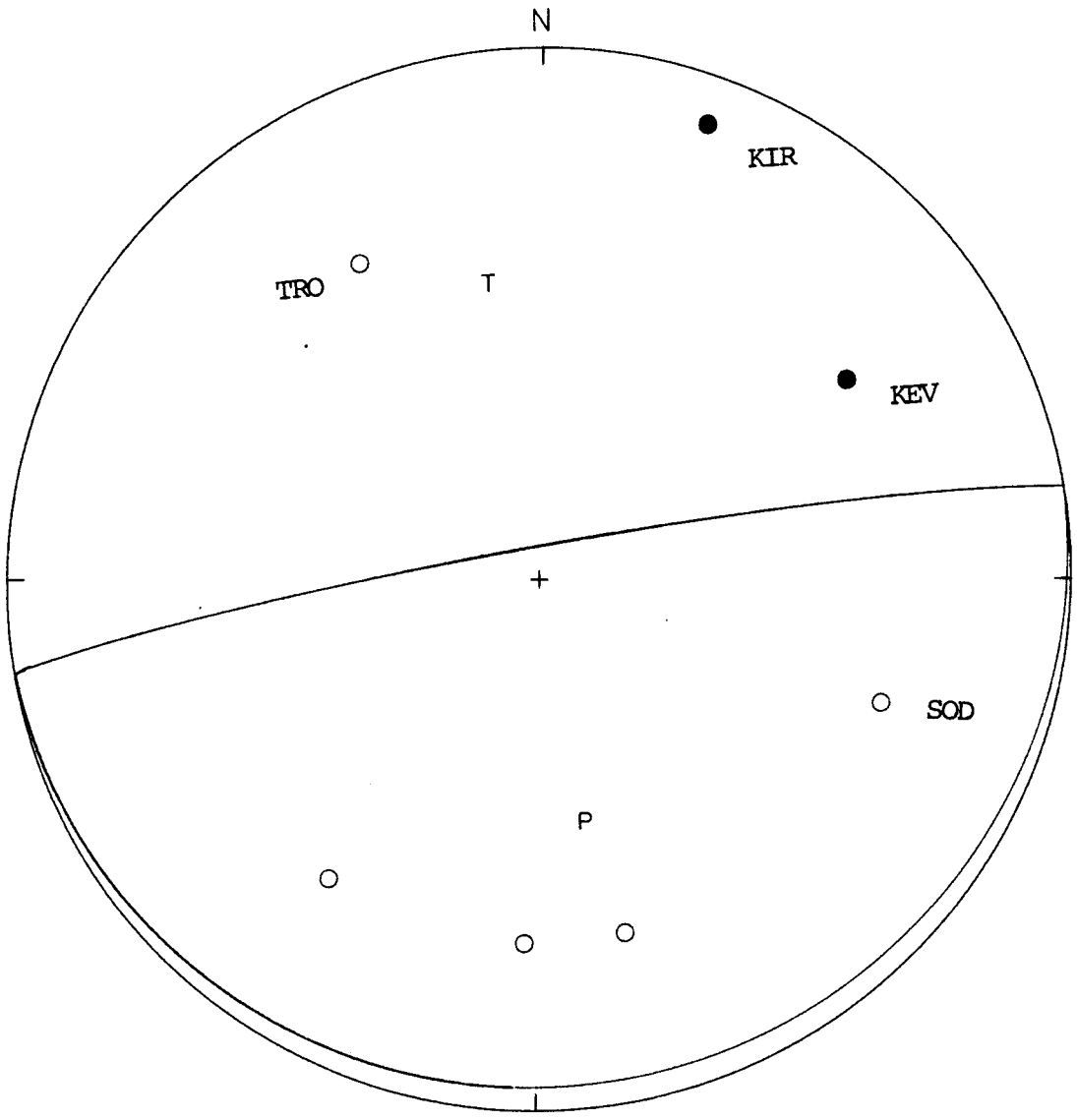

Figure 4-7. Focal mechanism for the event on 13 April 1967. Nodal planes and pressure (P) and tension (T) axes are shown on an equal-area lower hemisphere projection. Observed P-wave first motions are plotted with open circles and solid circles indicate clear positive first motion observed.

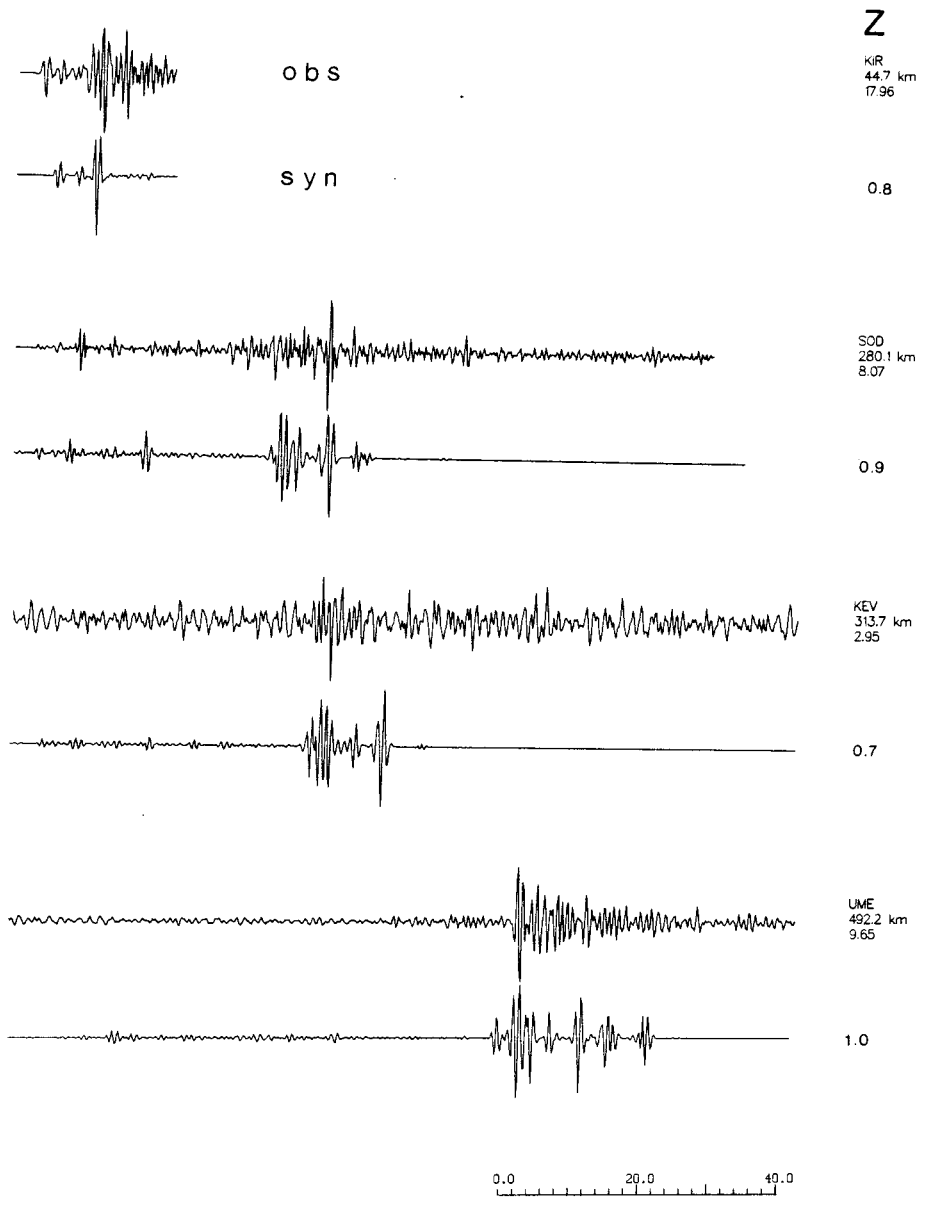

Figure 4-7a. Comparison of observed vertical-component records (upper traces) from the event on 13 Apr. 1967 with synthetic seismograms (lower traces). The numbers at the end of the synthetic traces indicate the ratio of the maximum amplitude of the synthetic trace to that of the observed trace. Note that the ramp type source time function with rise time of 0.2 s is used.

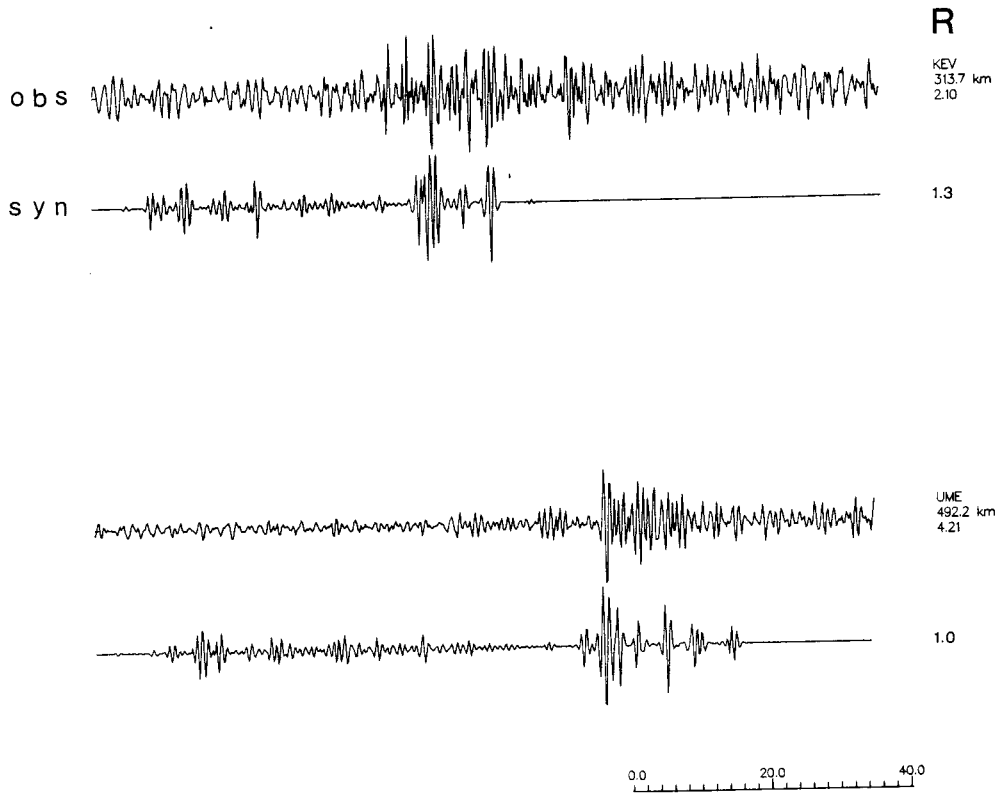

Figure 4-7b. Comparison of observed radial-component records (upper traces) from the event on 13 Apr. 1967 with synthetic seismograms (lower traces). Notations are the same as those in Figure 4-7a.

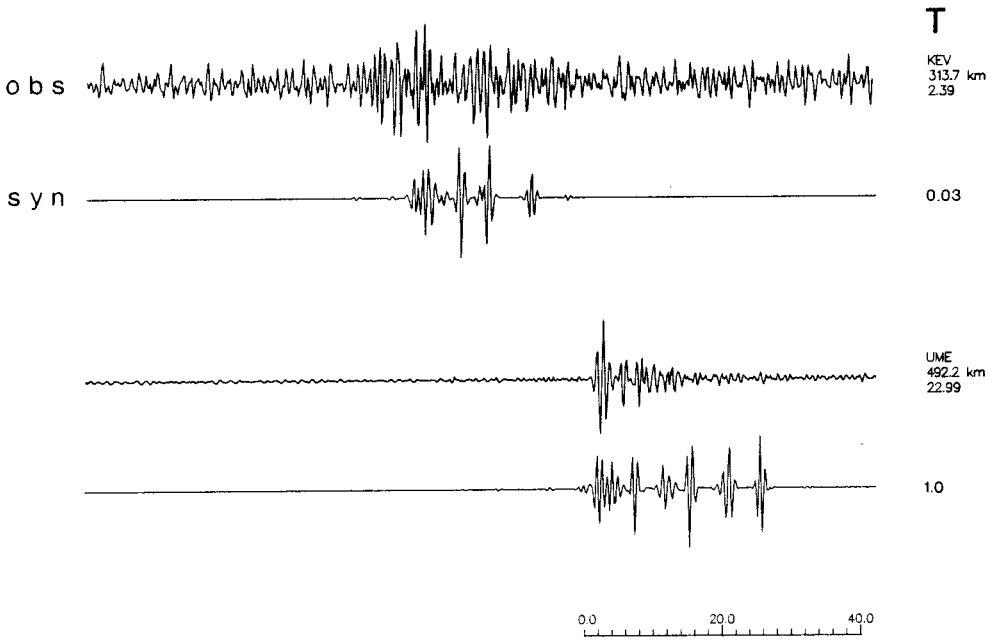

Figure 4-7c. Comparison of observed transverse-component records (upper traces) from the event on 13 Apr. 1967 with synthetic seismograms (lower traces). Notation are the same as those in Figure 4-7a.

The pressure axes is trending due south and has a plunge angle of 50^{o} SE, whereas the tension axis is trending due north and its plunge is 40^{o}NW.

A comparison of the vertical-component observed records and the final synthetic seismograms computed for the source mechanism parameters determined is shown in Figure 4-7a. As follows from the figure, the overall agreement of relative amplitudes and waveforms of the major phases between the observed and synthetic traces is fairly good, indicating that the source mechanism and focal depth estimates are reasonable.

Figures 4-7b and 4-7c exhibit the observed and synthetic radial and transverse components, respectively. These synthetic traces were computed with the same parameters as those used for the vertical-component synthetics. As in the previous event and the transverse component, the overall agreement between the observed and synthetic traces is rather poor. For the station KEV the relative amplitude between the prominent phases in the observed traces are not reproduced by the synthetics. This feature is most likely due to the bad quality of the original seismogram where the signal to noise ratio is very small.

5. DISCUSSION AND CONCLUSIONS

Epicenters of earthquakes relocated in this study propose the existence of a source region with the seismic activity clustered around Kiruna (centered at 68^{o}N and 20^{o}E). This source region is an elongate area about 70 km long and 20 km wide trending approximately NE (see Figure 2-1).

Despite some uncertainties, the relocated epicenters also indicate that most of the events in this source region might have occurred at focal depths between 15 and 25 km. Thus, hypocenters are likely near to the upper and lower crust boundary (Table 2-3).

At the western side of the region (around Kiruna), the seismicity appears to be more diffused, while at the eastern side there is a relatively clear alignment of the epicenters in roughly N-S direction (Figure 2-1). Relocation using the JHD places the hypocenters of the latter events at a depth of about 5 to 16 km (Table 2-3), which is also supported by the waveform modeling of the two largest events studied above.

The earthquakes in northern Sweden studied show nearly constant source radius of 0.4 - 0.6 km (Table 2-3), over the seismic moment range from 10^{20} to 10^{21} dyne-cm. This implies a steadily increasing stress drop with increasing seismic moment. This contradicts with constant stress drops for the large earthquakes worldwide (Kanamori & Anderson, 1975).

The source mechanisms obtained for the two largest earthquakes suggest that the mechanisms are dominated by a normal faulting on a near-vertical fault planes trending N-S to NE. Pressure axis is trending E-W almost perpendicular to the N-S aligned epicenters.

ACKNOWLEDGEMENTS

This work has been carried out at the Seismological Department, Uppsala University with financial support from the Swedish Nuclear Fuel and Waste Management Co (SKB) and the Swedish Natural Science Research Council under Grant G-GU-3164-137. We thank the director and colleagues at the Institute of Seismology, University of Helsinki, Finland for sending us copies and making available some original seismograms.

REFERENCES

Aki, K., 1980. Scattering and attenuation of shear waves in the lithosphere, J. Geophys. Res., **85**, 6496-6504.

Bollinger, G. A., 1979. Attenuation of the Lg phase and the determination of m_b in the Southeastern United States, Bull. Seism. Soc. Am., **69**, 45-63.

Bouchon, M., 1981. A simple method to calculate Green's functions for elastic layered media, Bull. Seism. Soc. Am., **71**, 959-971.

Brune, J. N., 1970. Tectonic stress and the spectra of seismic shear waves from earthquakes, J. Geophys. Res., **75**, 4997-5009.

Brune, J. N., 1971. Correction to "Tectonic stress and the spectra of seismic shear waves from earthquakes", J. Geophys. Res., **75**, 4997-5009.

Brune, J. N., Fletcher, J., Verson, F., Haar, L., Hank, T. and Berger, J., 1986. Low stress-drop earthquakes in the light of new data from Anza, California telemetered digital array, In: S. Das, J. Boatwright and C. H. Sholz (Editors), Earthquake Source Mechanics, Geophysical Monograph 37, Am. Geophys. Union, Washington, D. C., 238-245.

Bungum, H., Vaage, S. and Husebye, E. S., 1982. Meloy earthquake sequence, northern Norway: source parameters and their scaling relations, Bull. Seism. Soc. Am., **72**, 197-206.

Båth, M., 1971. Average crustal structure of Sweden, Pure. Appl. Geophys., **88**, 75-91.

Båth, M., 1979. Earthquakes in Sweden 1951-1976, Sveriges Geol. Unders., **72**, no. 12, 79pp.

Campillo, M., Bouchon, M. and Massinon, B., 1984, Theoretical study of the excitation, spectral characteristics and geometrical spreading of regional seismic phases, Bull. Seism. Soc. Am., **74**, 79-90.

Chun, K. Y., West, G. F., Kokoski, R. J. and Samson, C., 1987. A novel technique for measuring Lg attenuation - Results from Eastern Canada between 1 to 10 Hz, Bull. Seism. Soc. Am., **77**, 398-419.

Dainty, A. M., 1981. A scattering model to explain seismic Q observation in the lithosphere between 1 and 30 Hz, Geophys. Res. Lett., **8**, 1126-1128.

Dewey, J. W., 1983. Relocation of instrumentally recorded pre-1974 earthquakes in the south Carolina region, U. S. Geol. Survey Profes. Paper, 1313-Q, U. S. Government Printing Office, Washington.

Engdahl, E. R., Dewey, J. W. and Fujita, K., 1982. Earthquake location in island arcs, Phys. Earth Planet. Inter., **30**, 145-156.

Hasegawa, H. S., 1983. Lg spectra of local earthquakes recorded by the Eastern Canada Telemetered Network and spectral analysis, Bull. Seism. Soc. Am., **73**, 1041-1062.

Hasegawa, H. S., 1985. Attenuation of Lg waves in the Canadian Shield, Bull. Seism. Soc. Am., **75**, 1569-1582.

Herrmann, R. B. and Kijko, A., 1983. Modeling some empirical vertical component Lg relations, Bull. Seism. Soc. Am., **73**, 157-171.

Kanamori, H. and Anderson, D. L., 1975. Theoretical basis of some empirical relations in seismology, Bull. Seism. Soc. Am., Vol **65**, 1073-1095.

Keilis-Borok, V., 1959. On estimation of the displacement in an earthquake source and of source dimension, Ann. Geofis., **12**, 205-214.

Keilis-Borok, V., 1960. Investigation of the Mechanism of Earthquakes, Sov. Res. Geophys., **4**, Am. Geophys. Union, Consultants Bureau, New York, 201pp.

Kim, W. Y., 1987. Modelling short-period crustal phases at regional distances for the source parameter inversion, Phys. Earth Planet. Inter., **47**, 159-178.

Nuttli, O. W., 1983. Average seismic source parameter relations for mid-plate earthquakes, Bull. Seism. Soc. Am., **73**, 519-536.

Nuttli, O. W., 1986. Yield estimates of Nevada test site explosions obtained from seismic Lg waves, J. Geophys. Res., **91**, 2137-2151.

Slunga, R., Norrman, P. and Glans, A., 1984. Baltic shield seismicity, the results of a regional network, Geophys. Res. Lett., **11**, 1247-1250.

Street, R. L., Herrmann, R. B. and Nuttli, O. W., 1975. Spectral characteristics of the Lg waves generated by central United States earthquakes, Geophys. J. R. astr. Soc., **41**, 51-63.

Wiggins, R. a., 1976. Interpolation of digitized curves, Bull. Seism. Soc. Am., **66**, 2077-2081.

List of SKB reports

Annual Reports

1977–78
TR 121
KBS Technical Reports 1 – 120.
Summaries. Stockholm, May 1979.

1979
TR 79–28
The KBS Annual Report 1979.
KBS Technical Reports 79-01 – 79-27.
Summaries. Stockholm, March 1980.

1980
TR 80–26
The KBS Annual Report 1980.
KBS Technical Reports 80-01 – 80-25.
Summaries. Stockholm, March 1981.

1981
TR 81–17
The KBS Annual Report 1981.
KBS Technical Reports 81-01 – 81-16.
Summaries. Stockholm, April 1982.

1982
TR 82–28
The KBS Annual Report 1982.
KBS Technical Reports 82-01 – 82-27.
Summaries. Stockholm, July 1983.

1983
TR 83–77
The KBS Annual Report 1983.
KBS Technical Reports 83-01 – 83-76
Summaries. Stockholm, June 1984.

1984
TR 85–01
Annual Research and Development Report 1984
Including Summaries of Technical Reports Issued during 1984. (Technical Reports 84-01– 84-19)
Stockholm June 1985.

1985
TR 85-20
Annual Research and Development Report 1985
Including Summaries of Technical Reports Issued during 1985. (Technical Reports 85-01-85-19)
Stockholm May 1986.

1986
TR 86-31
SKB Annual Report 1986
Including Summaries of Technical Reports Issued during 1986
Stockholm, May 1987

1987
TR 87-33
SKB Annual Report 1987
Including Summaries of Technical Reports Issued during 1987
Stockholm, May 1988

Technical Reports

1988

TR 88-01
Preliminary investigations of deep ground water microbiology in Swedish granitic rocks
Karsten Pedersen
University of Göteborg
December 1987

TR 88-02
Migration of the fission products strontium, technetium, iodine, cesium and the actinides neptunium, plutonium, americium in granitic rock
Thomas Ittner[1], Börje Torstenfelt[1], Bert Allard[2]
[1]Chalmers University of Technology
[2]University of Linköping
January 1988

TR 88-03
Flow and solute transport in a single fracture. A two-dimensional statistical model
Luis Moreno[1], Yvonne Tsang[2], Chin Fu Tsang[2], Ivars Neretnieks[1]
[1]Royal Institute of Technology, Stockholm, Sweden
[2]Lawrence Berkeley Laboratory, Berkeley, CA, USA
January 1988

TR 88-04
Ion binding by humic and fulvic acids: A computational procedure based on functional site heterogeneity and the physical chemistry of polyelectrolyte solutions
J A Marinsky, M M Reddy, J Ephraim, A Mathuthu
US Geological Survey, Lakewood, CA, USA
Linköping University, Linköping
State University of New York at Buffalo, Buffalo, NY, USA
April 1987

TR 88-05
Description of geophysical data on the SKB database GEOTAB
Stefan Sehlstedt
Swedish Geological Co, Luleå
February 1988

TR 88-06
Description of geological data in SKBs database GEOTAB
Tomas Stark
Swedish Geological Co, Luleå
April 1988

TR 88-07
Tectonic studies in the Lansjärv region
Herbert Henkel
Swedish Geological Survey, Uppsala
October 1987

TR 88-08
Diffusion in the matrix of granitic rock. Field test in the Stripa mine. Final report.
Lars Birgersson, Ivars Neretnieks
Royal Institute of Technology, Stockholm
April 1988

TR 88-09
The kinetics of pitting corrosion of carbon steel. Progress report to June 1987
G P Marsh, K J Taylor, Z Sooi
Materials Development Division
Harwell Laboratory
February 1988

TR 88-10
GWHRT – A flow model for coupled groundwater and heat flow
Version 1.0
Roger Thunvik[1], Carol Braester[2]
[1] Royal Institute of Technology, Stockholm
[2] Israel Institute of Technology, Haifa
April 1988

TR 88-11
Groundwater numerical modelling of the Fjällveden study site – Evaluation of parameter variations
A hydrocoin study – Level 3, case 5A
Nils-Åke Larsson[1], Anders Markström[2]
[1] Swedish Geological Company, Uppsala
[2] Kemakta Consultants Co, Stockholm
October 1987

TR 88-12
Near-distance seismological monitoring of the Lansjärv neotectonic fault region
Rutger Wahlström, Sven-Olof Linder,
Conny Holmqvist
Seismological Depertment, Uppsala University,
Uppsala
May 1988

TR 88-13
Validation of the rock mechanics HNFEMP code against Colorado school of mines block test data
Ove Stephansson, Tomas Savilahti
University of Luleå, Luleå
May 1988

TR 88-14
Validation of MUDEC against Colorado school of mines block test data
Nick Barton, Panayiotis Chryssanthakis,
Karstein Monsen
Norges Geotekniske Institutt, Oslo, Norge
April 1988

TR 88-15
Hydrothermal effects on montmorillonite. A preliminary study
Roland Pusch
Ola Karnland
June 1988

TR 88-16
Swedish Hard Rock Laboratory
First evaluation of preinvestigations 1986-87 and target area characterization
Gunnar Gustafson
Roy Stanfors
Peter Wikberg
June 1988

TR 88-17
On the corrosion of copper in pure water
T E Eriksen[1], P Ndalamba[1], I Grenthe[2]
[1] The Royal Institute of Technology, Stockholm
Department of nuclear chemistry
[2] The Royal Institute of Technology, Stockholm
Department of inorganic chemistry
March 1988

TR 88-18
Geochemical modelling of the evolution of a granite-concrete-water system around a repository for spent nuclear fuel
Bertrand Fritz, Benoit Madé, Yves Tardy
Université Louis Pasteur de Strasbourg
April 1988

TR 88-19
A Bayesian nonparametric estimation of distributions and quantiles
Kurt Pörn
Studsvik AB
November 1988

TR 88-20

Creep properties of welded joints in OFHC copper for nuclear waste containment

Bo Ivarsson, Jan-Olof Österberg
Swedish Institute for Metals Research
August 1988

TR 88-21

Modelling uranium solubilities in aqueous solutions: Validation of a thermodynamic data base for the EQ3/6 geochemical codes

I Puigdomenech[1], J Bruno[2]
[1]Studsvik Nuclear, Nyköping
Environmental Services
[2]Royal Institute of Technology, Stockholm
Department of Inorganic Chemistry
October 1988

TR 88-22

Radiolysis of ground water: influence of carbonate and chloride on the hydrogen peroxide production

T E Eriksen[1], P Ndalamba[2], H Christensen[2],
E Bjergbakke[3]
[1]The Royal Institute of Technology, Department of Nuclear Chemistry, S-100 44 Stockholm, Sweden
[2]Studsvik Energiteknik AB, S-611 82 Nyköping, Sweden
[3]Risö National Laboratory, DK-4000 Roskilde, Denmark
December 1988